

Chapter 2

Characterization and Modeling of Lithium Dendrite Growth

Dendrites are a common occurrence when electrodepositing metals. Although the term “dendrite” is prevalent throughout the scientific literature when referencing Li deposition, such structures are atypical (i.e., in general, the plated Li morphology does not consist of regular branched, tree-like structures). Instead, Li tends to plate from solution as particles/nodules or whiskers/needles/filaments, which can aggregate into more complex constructs. Due to its ubiquitous usage for Li electrochemistry, however, the term “dendrite” will be used throughout the text in this book to refer to the latter structures. It is also notable that the literature that addresses the theory of Li electrodeposition has focused largely on the numerous determinant factors that influence classical dendritic metal plating, but the evolution of the plated Li structural characteristics is in actuality dictated to a great extent by the concurrent reactions between the reactive Li and electrolyte components (i.e., SEI formation).

2.1 Characterization of Lithium Dendrite Growth

As discussed in Chap. 1, the Li dendrite growth during the Li deposition process is a critical issue for the battery safety. Extensive efforts have been made to characterize and analyze the formation and growth processes of Li dendrites in order to reveal the mechanisms of dendrite formation and growth processes and then find the approaches to suppress or prevent the dendrite formation. In the last four decades, many different characterization methods have been used to study Li electrodes and the dendrite formation, including scanning electron microscopy (SEM) (Aurbach et al. 1998; Dollé et al. 2002), optical microscopy (Howlett et al. 2003; Nishikawa et al. 2010; Arakawa et al. 1993), atomic force microscopy (AFM) (Aurbach and Cohen 1997), transmission electron microscopy (TEM) (Liu et al. 2011; Ghassemi et al. 2011), nuclear magnetic resonance (NMR) (Chang et al. 2015), Fourier transform infrared spectroscopy (FTIR) (Morigaki 2002; Aurbach et al. 1987, 1995,

1997; Kanamura et al. 1997), and x-ray photoelectron spectroscopy (XPS) (Ota et al. 2004a; Aurbach et al. 1993; Kanamura et al. 1995b). Both morphology and chemical composition of the deposited Li metal films have been extensively investigated. The main approaches used in the characterization of electrochemically deposited Li metal films are briefly introduced in this chapter.

2.1.1 Characterization of Surface Morphologies

2.1.1.1 SEM

Among various observation methods, SEM is the most common and useful technique to examine Li electrode surface morphologies. Morphology study focuses on variation of the Li surface and formation of Li dendrites. Since the 1970s, this method has been used to study Li film growth (Dey 1976) both ex situ and in situ during dendrite growing/stripping processes (Ding et al. 2013, 2014; Zhamu et al. 2012; Ryou et al. 2012; Stark et al. 2011; Aurbach et al. 1989, 1990a, 1994b; Besenhard et al. 1987; Kanamura et al. 1995a; Yamaki et al. 1998; Shiraishi et al. 1999; Ota et al. 2004a; Gireaud et al. 2006; López et al. 2009; Nazri and Muller 1985b; Yoshimatsu et al. 1988; Choi et al. 2011; Lee et al. 2006; Yoon et al. 2008; Li et al. 2014a; Bieker et al. 2015). With its high resolution images, SEM is a powerful technique to analyze the surface change of Li metal during the deposition and stripping cycles. The effects of solvents (Aurbach et al. 1990a, b; Besenhard et al. 1987; Ota et al. 2004a; Bieker et al. 2015; Naoi et al. 1999), salts (Aurbach et al. 1994; Kanamura et al. 1995a; Yang et al. 2008), additives, (Shiraishi et al. 1999; Fujieda et al. 1994; Osaka et al. 1997b; Ota et al. 2004b; Lee et al. 2007), and other treatments (Stark et al. 2011; Thompson et al. 2011; Stark et al. 2013) have been directly discovered using SEM images. With the help of SEM observations, the correlation between the surface chemistry and morphology of Li electrodes was built (Aurbach et al. 1994), and the morphological transitions on Li metal anodes during cycling were examined (López et al. 2009). In the ex situ SEM studies, the Li samples have been transferred into the SEM instrument chamber in an inert atmosphere to avoid reaction of Li metal with ambient air as described by Kohl and coworkers (Stark et al. 2011). In the in situ SEM observation of Li dendrite formation, Orsini et al. (1998, 1999) first reported using in situ SEM to observe the cross section of plastic rechargeable Li batteries using solid polymer electrolytes. They observed the accumulation of mossy Li and growth of dendritic Li at the Li/polymer electrolyte (Fig. 2.1), which was the origin of rapid interface deterioration and capacity fading.

Neudecker et al. (2000) used in situ SEM to observe variation in the behavior of the anode current collector and the overlayer during Li deposition and stripping in an in situ built solid-state thin-film battery. The cross-sectional SEM image of the battery is shown in Fig. 2.2a. During the initial charge of the battery at 4.2 V, Li was plated between the anode current collector (i.e., Cu) and the solid-state

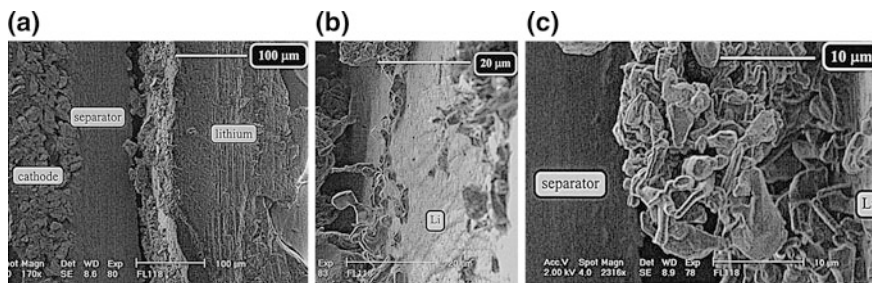


Fig. 2.1 **a** Cross section of a Li battery after one charge at 1C; **b** surface of the Li anode of a Li battery after one charge at 1C; **c** Li deposit on the Li surface after one charge at 1C. The 1C rate was 2.2 mA cm^{-2} . Reproduced with permission—Copyright 1998, Elsevier (Orsini et al. 1998)

electrolyte (i.e., lithium phosphorous oxynitride or LiPON), and lifted the Cu/LiPON overlayer but did not significantly penetrate the Cu film (Fig. 2.2b). During discharge to 3.0 V, the plated Li was stripped from the Cu substrate but the inactive Li prevented the exposed edge of the Cu/LiPON overlayer from completely settling onto the LiPON electrolyte again (Fig. 2.2c). Recently, Sagane et al. (2013) also reported use of in situ SEM to observe Li plating and stripping reactions at the LiPON/Cu interface. They found that nucleation reactions are the rate-determining step during the Li plating process, while the Li^+ cation diffusivity governs the stripping process.

Nagao et al. (2013) also used in situ SEM to study the Li deposition and dissolution mechanism in a bulk-type solid-state cell with a $\text{Li}_2\text{S-P}_2\text{S}_5$ solid-state electrolyte (SSE). They reported that at a deposition current density over

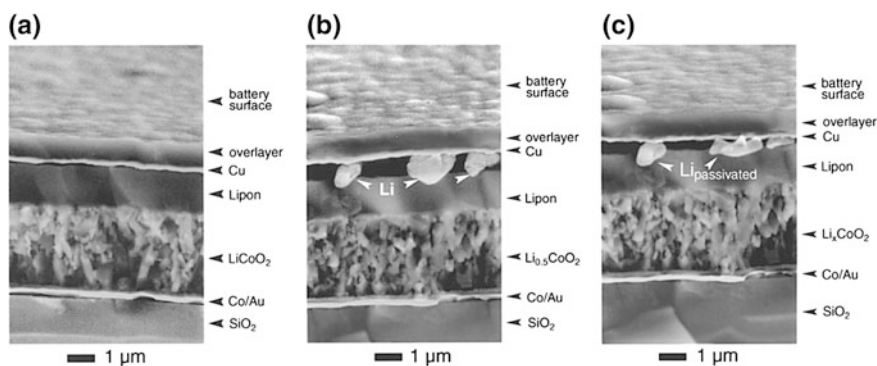


Fig. 2.2 In situ SEM micrographs showing cross-sectional views of a Li-free thin-film battery with an in situ plated Li anode: **a** 1 μm LiPON overlayer/2000 Å Cu anode current collector/1.5 μm LiPON electrolyte/3.0 μm LiCoO_2 cathode on quartz glass substrate prior to the initial charge, **b** same cell but at the end of the initial charge to 4.2 V, and **c** same cell but at the end of the first discharge to 3.0 V. The markers indicate a length of 1 μm. Reproduced with permission—Copyright 2000, The electrochemical society (Neudecker et al. 2000)

1 mA cm^{-2} , the local Li deposition triggered large cracks, resulting in a decrease in the reversibility of Li deposition and dissolution. On the other hand, at a low current density of 0.01 mA cm^{-2} , Li deposition was homogeneous thus greatly reducing the occurrence of unfavorable cracks, which enables reversible deposition and dissolution. These results suggest that homogeneous Li deposition on the surface of the SSE and suppression of the growth of Li metal along the grain boundaries inside the SSE are the keys to achieve the repetitive Li deposition and stripping without deterioration of the SSE. Clearly, SEM (either *ex situ* or *in situ*) is a very useful technique to investigate morphology variations of Li electrodes during deposition and stripping in open cells (Li et al. 2014a). However, because of the ultrahigh vacuum condition in SEM tests, most *in situ* SEM investigations of Li deposition/stripping processes are performed on batteries using solid polymer or inorganic SSE. It is still difficult to conduct an *in situ* observation of Li formation and growth in conventional liquid electrolytes, which is more relevant to most of practical applications.

2.1.1.2 Optical Microscopy

Optical microscopy is another way to observe the Li dendrites and it has been widely used as an *in situ* method to observe and record the Li dendrite growing/stripping processes under working conditions close to those of practical applications (Osaka et al. 1997a). Although the resolution of optical microscopy is not as high as that of SEM, it still could easily and instantaneously distinguish the surface change and dendrite formation. It is an intuitional observation on Li electrodes and very helpful to understand a continuous dendrite growing/stripping process. With digital recording devices, the dendrite formation process can be recorded as a video. Therefore, the optical microscopy technique has been widely used to analyze Li electrodes *in situ*. However, a special optical cell is needed for *in situ* optical study of Li dendritic growth. Usually, such a cell is homemade as described by Brissot et al. (1998). The optical cell could work as an airtight electrochemical cell, and the Li electrode surface could be observed by optical microscopy. In the *in situ* observation, optical microscopy is more often used to study the cross section of a Li electrode to observe the dendrite growth perpendicular to the surface of the Li electrode (Stark et al. 2013; Brissot et al. 1998, 1999b; Sano et al. 2011; Howlett et al. 2003; Hernandez-Maya et al. 2015). Figure 2.3 shows typical dendrites formed at different current densities during *in situ* optical microscopy study. At low current density (0.2 mA cm^{-2}), needle-like and particle-like dendrites are observed, while at higher current densities ($\geq 0.7 \text{ mA cm}^{-2}$), dendrites have a tree-like or bush-like shape. Figure 2.4 shows the evolution of Li dendrites observed in the inter-electrode space while the cell is being polarized (at 0.05 mA cm^{-2}). The needle-like dendrite grows on the negative electrode and finally contacts the positive electrode, causing short circuit of the cell.

Fig. 2.3 Typical dendrites obtained with different current densities: **a** $J = 0.2 \text{ mA cm}^{-2}$ (needle-like dendrites), **b** $J = 0.7 \text{ mA cm}^{-2}$ (tree-like dendrites), **c** $J = 1.3 \text{ mA cm}^{-2}$ (bush-like dendrites). Reproduced with permission—Copyright 1998, Elsevier (Brissot et al. 1998)

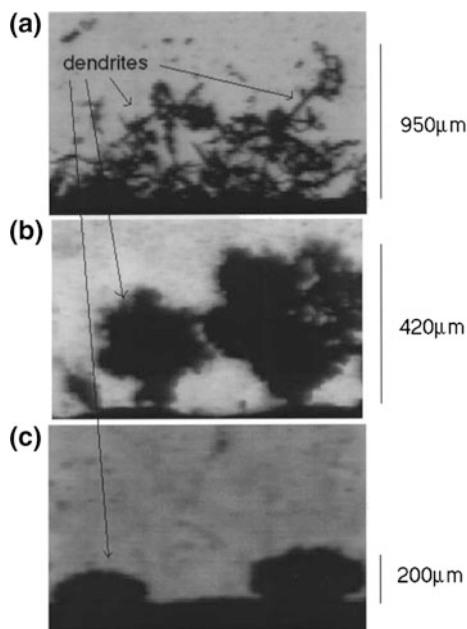
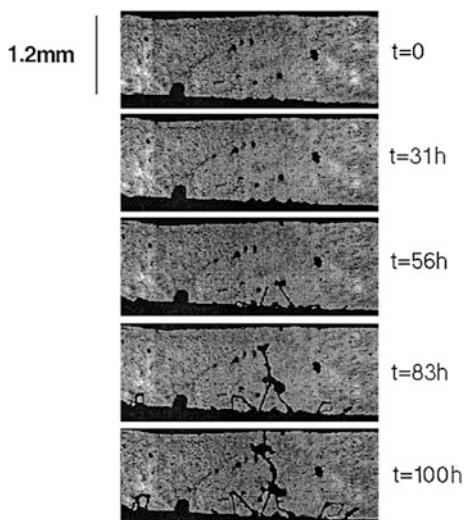


Fig. 2.4 Time variation of the dendrites observed in the inter-electrode space while polarizing the cell with $J = 0.05 \text{ mA cm}^{-2}$. Dendrites are seen to be needle-like. It shows that the dendrite grows on negative electrode with time and finally contacts the positive electrode, causing short circuit of the cell. Reproduced with permission—Copyright 1999, Elsevier (Brissot et al. 1999b)



2.1.1.3 AFM

AFM is another useful technique to investigate Li electrode morphology. The resolution of AFM is much better than that of optical microscopy. At the same time, AFM can give a three-dimensional (3D) morphology image that is difficult to get

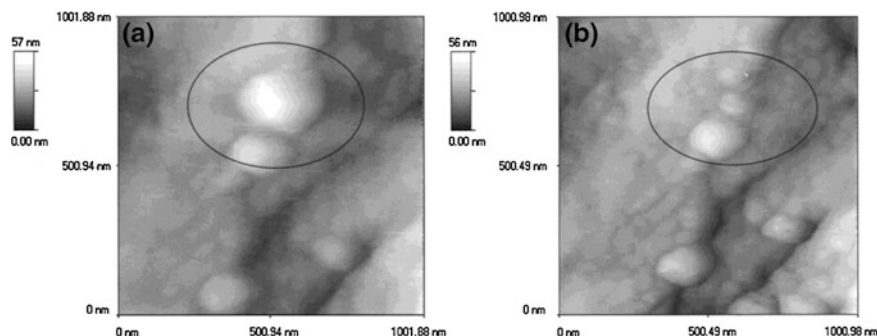


Fig. 2.5 AFM images ($1 \times 1 \mu\text{m}$) of a Li electrode in a 0.5 M LiAsF₆/PC solution. **a** an image obtained after Li deposition, 0.41 C cm^{-2} . New Li deposits are marked by a circle. **b** an image of the same area after consecutive Li dissolution (0.41 C cm^{-2}). The same area marked in **a** is also circled here. Reproduced with permission—Copyright 2000, American Chemical Society (Cohen et al. 2000)

from SEM or optical microscopy. In 1996, Aurbach and Cohen first used AFM to study the Li deposition processes in nonaqueous electrolyte systems (Aurbach and Cohen 1996). In that work, the basic electrochemical cell was modified to hold the highly sensitive electrodes and electrolyte solution and to isolate them from atmospheric contaminants. They found that the AFM scanning is not destructive and does not change the morphology on the surface. After that, more work (Morigaki and Ohta 1998; Aurbach et al. 1999; Cohen et al. 2000; Morigaki 2002; Mogi et al. 2002a, b, c) using in situ AFM was conducted. With the special 3D morphology of AFM images, the swelling and shrinking of Li surfaces during Li deposition and stripping processes have been discovered (Morigaki 2002). Figure 2.5 shows AFM images of a Li surface film deposited in a 0.5 M LiAsF₆/propylene carbonate (PC) electrolyte, where (a) a bump after Li deposition and (b) shrinkage after consecutive Li stripping are clearly seen (Morigaki 2002). Moreover, investigation by AFM has revealed that the structure of the Li surface consists of grain boundaries, ridge lines, and flat areas (Morigaki and Ohta 1998), which cannot be proven by other morphology test methods including SEM and optical microscopy. Based on these findings, the breakdown and reparation of the SEI films on Li electrodes during Li deposition/stripping cycles have been proposed (Fig. 2.6) and probed (Aurbach and Cohen 1996; Cohen et al. 2000).

Several modified AFM methods have also been used in the characterization of Li film deposition. Shiraishi et al. reported using in situ fluid tapping-mode AFM (TMAFM) coupled with an electrochemical quartz crystal microbalance to investigate the electrochemical stripping behavior of Li metal in nonaqueous electrolytes containing a small amount of HF (Shiraishi and Kanamura 1998), and also using TMAFM with surface potential microscopy (SPoM) to study the surface condition of the electrodeposited Li on a Ni substrate (Shiraishi et al. 2001). Recently, Zhang et al. (2014) used amplitude-modulated electrostatic force microscopy (AM-EFM) (a special type of AFM) to study the surfaces of deposited Li films. The Li films

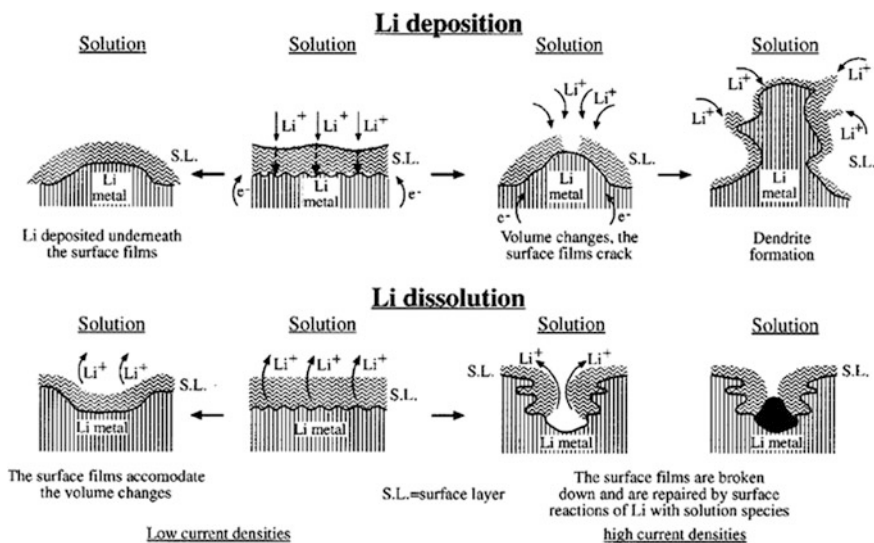


Fig. 2.6 A description of the morphology and failure mechanisms of Li electrodes during Li deposition and dissolution illustrating selected phenomena: the beginning of dendrite formation (*top*) and nonuniform Li dissolution accompanied by breakdown and reparation of the surface films (*bottom*). Reproduced with permission—Copyright 2000, American Chemical Society (Cohen et al. 2000)

were electrodeposited for 15 h on Cu foils in electrolytes of 1 M LiPF_6 -PC without and with 0.05 M CsPF_6 additive. Li dendrites were formed in the control electrolyte (i.e., without Cs^+ additive) and a smooth Li film was obtained in the Cs^+ containing electrolyte. As shown in Fig. 2.7, the EFM images recorded at a probe voltage of -1 V for the Li film formed in the control electrolyte exhibit wide color variations or a strong contrast, which indicates a large fluctuation and nonuniform distribution of electric field across the detected Li surface. In comparison, the EFM image for the Li film formed in the Cs^+ -containing electrolyte shows narrow color variations or relatively small contrast, indicating a uniform distribution of the electric field across the Li surface and is consistent with a smooth Li film.

2.1.1.4 TEM

Due to the success of the application of optical microscopy in the observation of morphologies of deposited Li films in microscale, another electron microscopy, i.e., in situ TEM, was recently used to observe in real time the formation of Li fibers or Li dendrite growth at nanoscale (Liu et al. 2011; Ghassemi et al. 2011). Huang and coworkers first reported the direct observation of Li fiber growth on different nanowire anodes (such as silicon or tin oxide) during in situ charging of nanoscale Li-ion batteries inside a TEM (Huang et al. 2010). Li fibers of up to 35 μm long

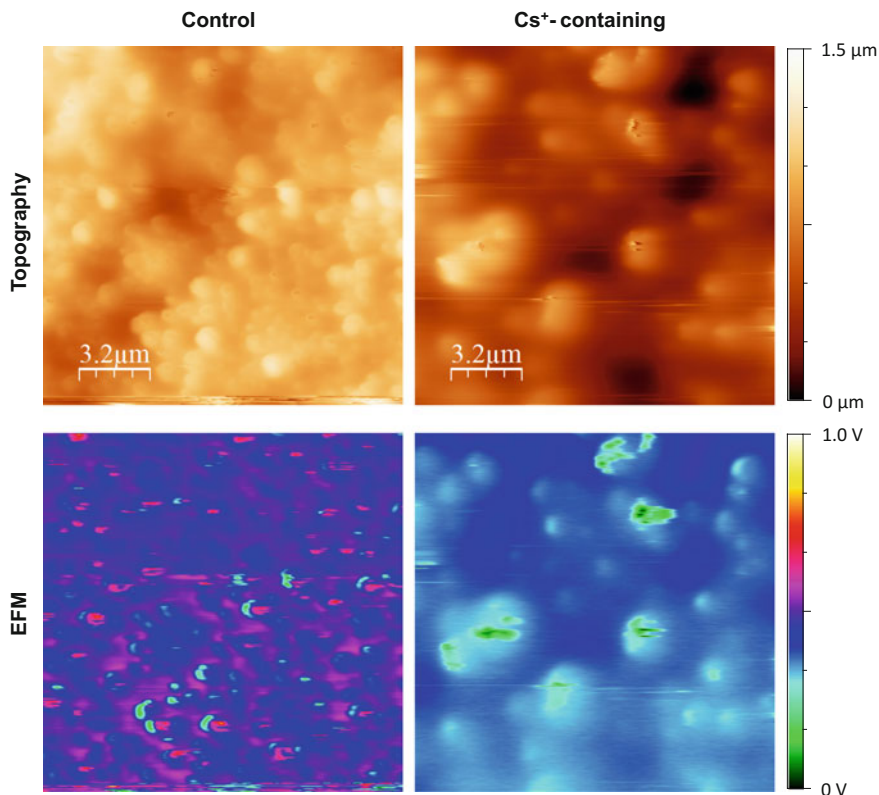


Fig. 2.7 Topography and EFM images (recorded at a probe voltage of -1 V and frequency of 22 kHz) of a dried Li film after deposition from the control electrolyte without Cs^+ -additive (i.e., 1.0 M LiPF_6/PC) and the Cs^+ -containing electrolyte (i.e., 1.0 M $\text{LiPF}_6\text{-PC}$ with 0.05 M CsPF_6). The EFM images show the distribution of electric field across the Li surface. The *wide color* variations in the EFM images obtained in the control electrolyte indicate a nonuniform distribution, while the *narrow color* variations exhibited in the images obtained in Cs^+ -containing electrolyte indicate a more uniform distribution of electric field across the detected Li surface. Reproduced with permission—Copyright 2015, American Chemical Society (Zhang et al. 2014)

grew on nanowire tips along the nanowire axis in an ionic liquid (IL)-based electrolyte. After that, Yassar and coworkers also used this in situ TEM technology to study the growth of Li dendrites (Ghassemi et al. 2011). They reported clear observation of nucleation of Li^+ cations at the anode/electrolyte interface and then growth of Li fibers or Li dendrites on the anode surface in a nanoscale Li-ion battery (Fig. 2.8). In situ TEM is a very promising method to observe and study Li dendrite growth in situ during the continuous charging/discharging processes of a battery, especially at the nanoscale.

Although in situ TEM images have been used to reveal the formation and growth of Li dendrites during the continuous charging/discharging processes of a battery, an IL

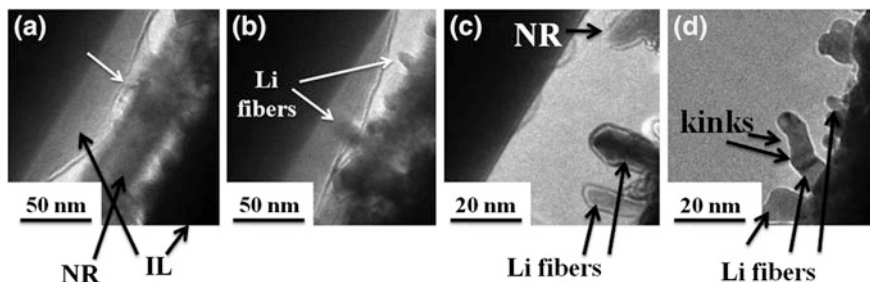


Fig. 2.8 **a** Black arrows indicate an individual silicon nanorod surrounded by ionic liquid. **b** Arrows indicate the formation of Li islands on the nanorod. **c** Represents the growth of Li fibers. **d** The formation of kinks and growth of Li fibers are marked by black arrows. Reproduced with permission—Copyright 2011, American Institute of Physics (Ghassemi et al. 2011)

electrolyte or an SSE has to be used in most in situ TEM studies because the high vapor pressure of a practical liquid electrolyte is not compatible with the high vacuum required by a conventional TEM system. It is well known that an SEI layer formed on the surface of a Li film or dendrite is critical for Li deposition/stripping. However, the SEI formed in IL or SSE is greatly different from those formed in the conventional electrolytes used in Li metal batteries. Therefore, the interaction between Li dendrites and a practical liquid electrolyte still cannot be observed in these in situ TEM studies. Very recently, with the development of liquid cells for in situ TEM techniques, a true operando TEM investigation on Li dendrite growth has been performed in electrochemical cells with conventional liquid electrolytes for Li-ion batteries (Gu et al. 2013; Mehdi et al. 2014, 2015; Sacci et al. 2014). Sacci et al. (2014) reported the direct visualization of an initial dendritic SEI formation prior to Li deposition, and this dendritic morphology remained on the surface after Li dissolution during the in situ electrochemical TEM study, which used 1.2 M LiPF_6 in ethylene carbonate (EC)/dimethyl carbonate (DMC) (3:7 by wt) as electrolyte. Mehdi et al. (2015) used in situ electrochemical scanning TEM (STEM) to study the initial stages of SEI formation and Li dendrite evolution at the anode/electrolyte interface during Li deposition/stripping processes in 1 M LiPF_6/PC electrolyte. The high-angle annular dark field (HAADF) STEM images of the anode/electrolyte interface during the first three charge-discharge cycles of this operando Li battery are shown in Fig. 2.9. The deposition and stripping of Li is clearly observed. Some electrochemically inactive or “dead” Li residues around the electrode after Li stripping for all the three cycles are present, which are no longer attached to the Pt electrode.

Presently, the liquid cell TEM gives relatively lower resolution images than the open cell (i.e., vacuum conditioned) TEM does due to the limitation of cell thickness required to hold liquid electrolyte. Therefore, future improvement is required on the liquid cell fabrication (including electrodes with different alloying performance and control of the thickness) along with use of faster imaging methods. Such improvements should enable the clear observations of the initial stages of different mechanisms to be quantified on the nanometer to atomic scale. When

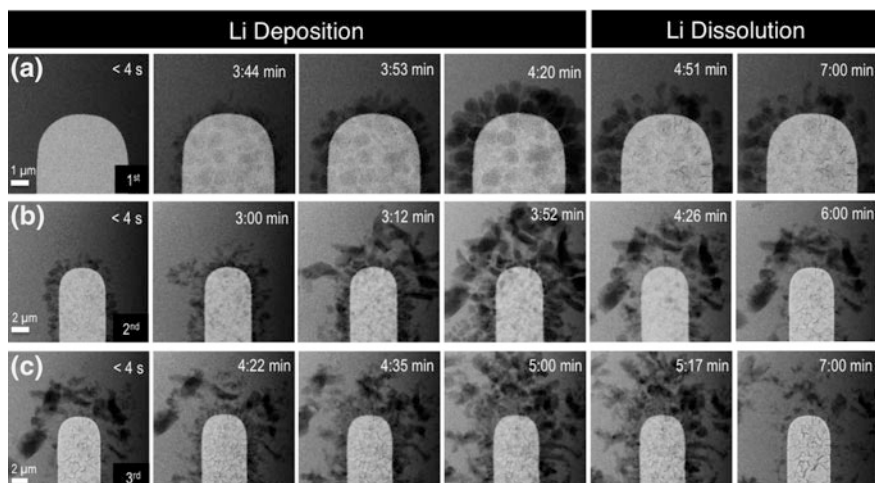


Fig. 2.9 HAADF images of Li deposition and dissolution at the interface between the Pt working electrode and the $\text{LiPF}_6\text{-PC}$ electrolyte during the **a** first, **b** second, and **c** third charge/discharge cycles of the operando cell. The formation of the SEI layer (ring of contrast around the electrode), alloy formation due to Li^+ ion insertion, and the presence of “dead Li” detached from the electrode can all be seen in the images at the end of the cycle, thereby demonstrating the degree of irreversibility associated with this process. Reproduced with permission—Copyright 2015, American Chemical Society (Mehdi et al. 2015)

coupled with different electrolyte compositions (i.e., solvents, salts, and additives), the improved liquid cell TEM technology may provide critical insights into the complex interfacial reactions for future Li-based and other next-generation energy storage systems.

2.1.1.5 NMR

NMR is a powerful tool for detecting chemical bonds or atomic surroundings. Recently, Bhattacharyya and Grey et al. proposed using the difference between NMR signal intensities of bulk and porous Li to identify the Li dendrite growth (Bhattacharyya et al. 2010). They have successfully used this method as an in situ tool to quantitatively observe the formation of Li dendrites in different electrolytes. Chandrashekar et al. (2012) reported using ^7Li magnetic resonance imaging (MRI) technique to detect in situ the variation of Li electrode morphologies during charge and discharge processes of a symmetric Li metal cell. The ^7Li NMR spectra of the Li metal resonance before (pristine) and after applying a current (charged) indicated that the area of the spectrum in the charged state was 2.3 times larger than that in the pristine state. This increase could be attributed to the formation of

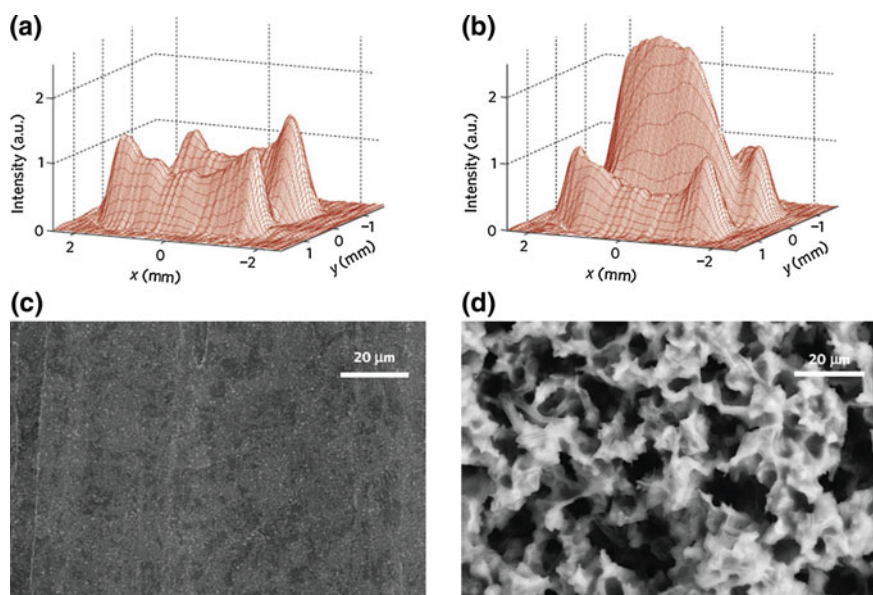


Fig. 2.10 ^7Li 2D MRI x-y images (frequency encoding in x and phase encoding in y) in the states of pristine (a) and after charging (b), and the related SEM images of Li anode in pristine (c) and charged (d) states. Reproduced with permission—Copyright 2012, Macmillan Publishers (Chandrashekar et al. 2012)

dendritic, mossy, and other microstructural metallic Li during charging. The two-dimensional ^7Li MRI images before and after the cell charging are depicted in Figs. 2.10a, b, where the cumulative signals were projected along the z direction which is perpendicular to the substrate. The MRI image of the charged battery revealed the negative electrode had a significant increase in signal of almost double, while the positive electrode showed a decrease in signal of about 23 % after charging. It indicated the location and change of microstructural Li morphology, which is consistent with findings from SEM images (Figs. 2.10c, d). Recently, Arai et al. (2015) used in situ solid-state ^7Li NMR to observe Li metal deposition during overcharge in Li-ion batteries. Hu et al. also used in situ NMR and computational modeling to investigate the role of Cs^+ additive (Hu et al. 2016). These works indicate that NMR not only can detect the morphology variation during the Li metal deposition process, but also can reveal the possible composition of SEI layers formed on the surfaces of Li films during the electrode plating process. By combining NMR and other characterization techniques, a more comprehensive understanding of the electrode plated Li films can be obtained.

2.1.2 Characterization Methods for Surface Chemistry

2.1.2.1 FTIR

The characterization methods discussed in the previous sections mainly provide information on the morphology variations of Li depositions. Several other methods have been used to analyze the chemical compositions of the surface films formed on the surface of deposited Li. The chemical composition of the Li surface film is strongly related to the electrolyte components. In turn, the SEI film formed on the surface of a Li deposition strongly affects the Li morphology and cycling performance of a Li metal battery (Aurbach et al. 1994). In this aspect, FTIR and XPS are widely used in this field to analyze the Li surface chemistry; FTIR is more suitable for detecting the organic components, while XPS gives more information about the inorganic components.

Since the 1980s, FTIR has been widely used to analyze the Li surface as a nondestructive method (Morigaki 2002; Aurbach et al. 1987, 1995, 1997; Kanamura et al. 1997). In the early years, FTIR was used as an ex situ method (Aurbach et al. 1987), but it was later developed as an in situ technique to analyze Li films during electrochemical processes (Morigaki 2002; Kanamura et al. 1997). FTIR has been used to investigate the influences of electrolyte solvents, salts, additives, and other contaminants on the Li surface. From the locations and strengths of the peaks in FTIR spectra, different chemical bonds or components on the Li electrode surface could be identified. An example is shown in Fig. 2.11 which shows FTIR spectra of Li electrodes prepared and stored for three days in EC-DMC solutions of 1 M LiAsF₆, LiPF₆, or LiBF₄ as indicated. A spectrum of a Li electrode prepared and stored in DMC containing 0.1 M CH₃OH is also presented for comparison (Aurbach et al. 1997).

2.1.2.2 XPS

It should be noted that although the FTIR technique is very useful to identify the surface components, it is limited in that it detects only the IR-active species and it cannot give the relative importance of each surface component and composition that affect the Li deposition morphology and battery performance. Therefore, other surface characterization methods and technologies besides FTIR are needed to get more detailed surface chemistry data on Li anodes. As mentioned above, XPS is another very useful tool to analyze the surface chemistry of Li electrodes; in particular, it gives more information about the elemental or inorganic components—data that FTIR cannot detect. Normally, as indicated from XPS and FTIR data by Aurbach et al. (1987), the major species in a Li surface film include Li₂O, LiOH, LiF, Li₂CO₃, lithium alkylcarbonate (RCOOLi), and hydrocarbon. Recently,

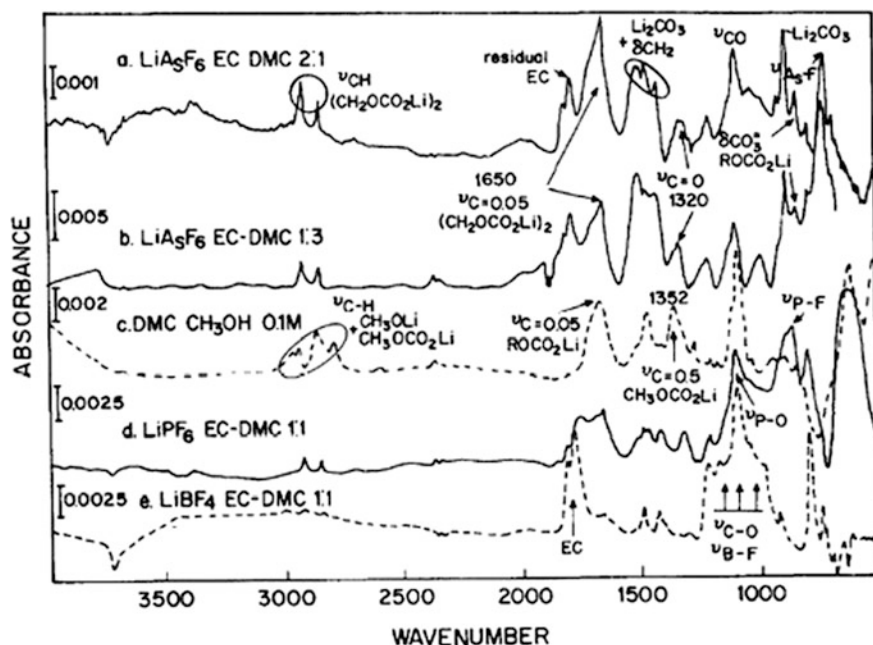


Fig. 2.11 FTIR spectra of Li electrodes prepared and stored for three days in EC-DMC solutions of 1 M LiAsF₆, LiPF₆, or LiBF₄ as indicated. A spectrum of a Li electrode prepared and stored in DMC containing 0.1 M CH₃OH is also presented for comparison. Reproduced with permission—Copyright 1997, Elsevier (Aurbach et al. 1997)

Wenzel et al. (2015) used the in situ XPS technique to study the stability of an SSE in contact with Li metal. The key concept was to use the internal Ar ion sputter gun in a standard lab-scale photoelectron spectrometer to deposit thin metal films (e.g., Li) on the sample surface and to study the reactions between metal and SSE by photoelectron spectroscopy directly after deposition (Fig. 2.12). This approach could give information on interfacial reactions and the interfacial kinetics, especially for the interface between the alkali metal and solid electrolyte in solid-state batteries.

With XPS analysis, the effects of different electrolyte solvents (Ota et al. 2004a; Aurbach et al. 1993; Kanamura et al. 1995b), lithium salts (Kanamura et al. 1995a; Fujieda et al. 1994), and additives (Shiraishi et al. 1999; Odziemkowski et al. 1992) on the Li surface chemistry have been investigated. Based on these data, especially with the vacuum etching technology of the XPS technique, not only the components but also the structural composition evolution of the SEI film can be revealed by XPS analysis (Ding et al. 2014; Kanamura et al. 1995a; Shiraishi et al. 1999; Zhang et al. 2014; Aurbach et al. 1993; Qian et al. 2015a, b).

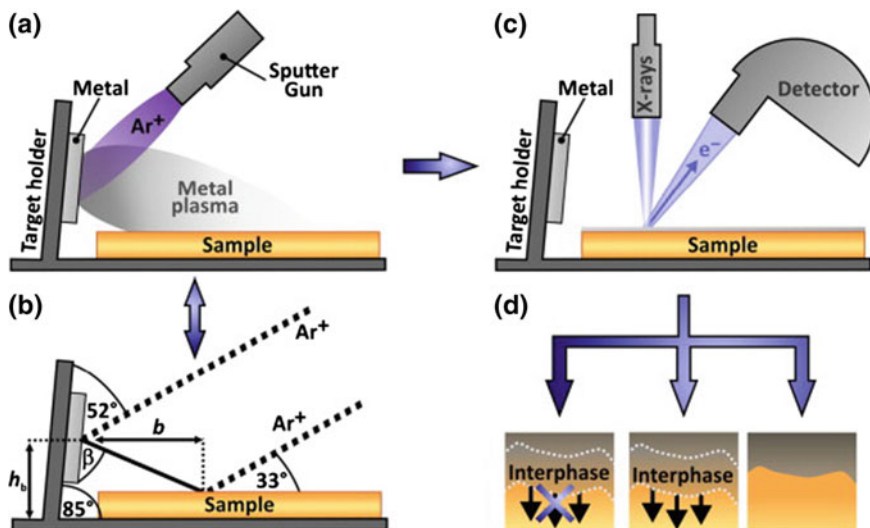


Fig. 2.12 The basic concept and setup of the in situ XPS technique. An argon ion beam is used to sputter lithium, gold or aluminum metal on the sample surface (a). In (b) the geometry is schematically shown. After deposition, the reaction products formed at the interface (d) are investigated using photoelectron spectroscopy, as shown in (c). Reproduced with permission—Copyright 2015, Elsevier (Wenzel et al. 2015)

2.1.3 Other Characterization Techniques

In addition to the methods discussed in the above sections, several other methods, including Raman spectroscopy (Raman) (Kominato et al. 1997), Auger electron spectroscopy (AES) (Ota et al. 2004a; Morigaki and Ohta 1998; Aurbach et al. 1993), and NMR (Kominato et al. 1997) have been used to analyze the surface chemistry of electroplated Li films. So far, attempts to use Raman spectroscopy to identify the surface films on the Li metal/electrolyte interphase have not been very successful. Only a few papers reported the Raman studies (Howlett et al. 2003; Rey et al. 1998a, b; Naudin et al. 2003). For example, Irish et al. used a Raman microprobe to study both in situ and ex situ the surface films formed on Li metal in contact with electrolytes of $\text{LiAsF}_6/\text{tetrahydrofuran}$ (THF) and $\text{LiAsF}_6/2\text{MeTHF}$ (Odziemkowski et al. 1992). The reaction products detected were mainly polytetrahydrofuran, some arsenolite (As_2O_3), and arsenious oxyfluorides $\text{F}_2\text{As-O-AsF}_2$. Raman technology might be expected to yield results similar to those of FTIR spectroscopy, but this technology is more complicated to use than FTIR (Odziemkowski et al. 1992). In addition, as indicated by Naudin et al. (2003), local heating of the samples under laser irradiation is unavoidable in Raman tests. The carbonate species on Li surface could be transformed into lithium acetylides of Li_2C_2 type, which gives a vibration peak of $\text{C}\equiv\text{C}$ at about 1845 cm^{-1} , thus giving a

faulty result to the interpretation. Therefore, the destructive effect of Raman laser beam on Li surfaces limits its use in the analysis of Li surface films.

Aurbach et al. (1993) used AES to measure the Li surface after the Li was immersed in an electrolyte of 0.2 M LiAsF₆/1,2-dimethoxyethane (DME) for 15 min followed by pure DME rinsing. They found that the AES spectra were similar to those seen with XPS. Carbon and oxygen were detected at the Li surface. With sputtering, the intensity of the carbon Auger peak decreased while the oxygen peak increased when compared to their initial peaks. It was suggested that the surface films of Li treated in DME consisted of two layers, the upper layer being an alkoxide film (probably LiOCH₃) and the layer close to Li being a mixture of Li₂O and LiOH. Kominato et al. (1997) also used AES to detect the surface compounds of Li after it was immersed in three electrolytes of EC/DMC with LiPF₆, LiClO₄, or LiTFSI. Except for LiF found in the Li surface film from the LiPF₆-based electrolyte, all major components in the three Li surfaces were Li–O components indicating LiOH, Li₂O, or other lithium oxide compounds. Morigaki and Ohta used scanning AES to analyze the Li surface in 1 M LiClO₄/PC solution also used AES to detect the surface compounds of Li after it was immersed in three electrolytes of EC/DMC with LiPF₆, LiClO₄, or LiTFSI. Except for LiF found in the Li surface film from the LiPF₆-based electrolyte, all major components in the three Li surfaces were Li–O components indicating LiOH, Li₂O, or other lithium oxide compounds. Morigaki and Ohta (1998) used scanning AES to analyze the Li surface in 1 M LiClO₄/PC solution. Li₂CO₃, Li₂O, and LiOH were localized on the ridge lines and the grain boundaries of the Li surface. AES technology can provide some useful information about the Li surface components, but it is very close to that obtained from XPS analysis. In addition, the AES equipment is more difficult to access than XPS equipment, so AES analysis has been used less frequently in Li metal investigations.

NMR has also been used to study the Li surface chemistry. Ota et al. (2004a, c) used NMR technology (¹H, ¹³C and 2D spectra) to analyze the surface components of deposited Li by dissolving the surface film in anhydrous dimethyl sulfoxide (DMSO)-d₆ and then recording the NMR spectra of the organic species in the DMSO-d₆ solution. They found that the organic surface layer on Li metal included lithium ethoxide, lithium ethylene dicarbonate, PEO, and lithium ethylene containing an oxyethylene unit. This is an indirect method to analyze the Li surface focusing on the dissolvable organic species. The obvious limitation of this technique is the inability to analyze the insoluble inorganic compounds formed on Li surfaces.

Nazri and Muller used secondary ion mass spectrometry (SIMS) to study the surface layer formed on electrochemically deposited Li on copper in a 1 M LiClO₄-PC electrolyte (Nazri and Muller 1985b). The obtained SIMS spectrum was complex and was difficult to interpret. Basically, the low mass range showed the fragments of PC, the salt, and water, while the high mass range indicated the presence of a polymeric material based on PC, a partially chlorinated hydrocarbon polymer, and their lithium adducts. The authors also applied the in situ x-ray diffraction (XRD) technique to the analysis of the formed Li surface films (Nazri

and Muller 1985a, b, c). The presence of Li_2CO_3 , Li_2O , and polymer compounds was also detected.

Temperature-programmed decomposition mass spectroscopy (TPD-MS) and gas chromatography–mass spectrometry (GC-MS) technology were also used by several groups to analyze the surface components of Li electrodes (Matsuda et al. 1995). Kominato et al. (Morigaki and Ohta 1998; Kominato et al. 1997) reported that the gases generated from Li films pretreated in EC-dimethyl carbonate (DMC) based electrolytes were mainly CH_4 , H_2O , CO , CH_3OH , CO_2 , and ethylene oxide. N_2 was also detected if LiTFSI was used as the electrolyte salt. The GC-MS detected the same gas components. This indicated that the detected gases were generated from the organic Li compounds that were the reaction products of Li and solvents (EC and DMC) and included lithium ethylene dicarbonate and lithium methylcarbonate. Ota et al. (2004a, c) also used GC-MS to investigate the Li surface compounds generated in EC/THF electrolytes. C_2H_4 , CO_2 , and C_2H_6 were detected and were mainly from the reductive components of EC. During TPD-MS and GC-MS measurements, the Li electrodes with the detected surface films need to be heated to give off the gases to be tested. The data from these MS measurements could provide more information on the Li surface film chemistry and support the results of other film measurements, such as FTIR and XPS.

Ota et al. (2004a, c) used ion chromatography (IC) to quantitatively analyze the Li surface films. The Li films were first dissolved in high-purity water and then tested by an IC instrument. By analyzing the contents of F^- , CO_3^{2-} , and Li^+ ions, quantitative information about the Li surface films could be obtained. They found that the Li surface film in EC-based electrolytes consisted mainly of lithium alkyl carbonate, and LiF content in the films formed in an electrolyte containing lithium imide salt was lower than those formed in the electrolytes containing LiPF_6 salt.

The in situ scanning vibrating electrode technique has also been used to map the surface electric field of Li electrodes (Matsuda et al. 1995; Ishikawa et al. 1997). The surface electric field on a Li electrode is based on its morphology and composition uniformity. So this technology reflects not only the surface morphology, but also the chemical composition uniformity of the Li surface. However, because the scanning step of this technology is not small enough, the definition obtained using this technology is not satisfactory.

In a recent effort, Harry et al. (2014, 2015) used synchrotron hard x-ray microtomography to investigate the failure caused by dendrite growth in high-energy density, rechargeable batteries with Li metal anodes. When a symmetric $\text{Li}|\text{polymer electrolyte}|\text{Li}$ cell was cycled at 90°C , they found that the bulk of the dendritic structure lay within the electrode, underneath the polymer/electrode interface, during the early stage of dendrite development. Furthermore, they observed crystalline impurities, present in the uncycled Li anodes, at the base of the subsurface dendritic structures. The portion of the dendrite protruding into the electrolyte increases on cycling until it spans the electrolyte thickness, causing a short circuit. Contrary to conventional wisdom, it seems that preventing dendrite formation in polymer electrolytes depends on inhibiting the formation of subsurface structures in the Li electrode. These results demonstrate that x-ray

microtomography is another powerful tool to provide a clear failure mechanism in Li metal batteries.

In summary, characterization of morphologies and surface components of electroplated Li anodes is a complicated task. SEM and FTIR/XPS are the most common methods used to investigate the surface morphology and chemistry, respectively, of the electrodeposited Li films. Many other methods discussed in this chapter also provide valuable information on Li films. However, no single technique is enough to provide comprehensive understanding of the studied Li films, especially for the surface reaction products or SEI layer formed on a Li film. Therefore, a combination of multiple characterization and analysis methods is required to have a good understanding of the properties of electrodeposited Li films.

2.2 Effect of SEI Layer on Lithium Dendrite Growth

Various models proposed in the literature have provided important guidance on the nucleation and growth of metal dendrites, especially for metals that do not react with electrolyte in a significant way. However, Li is thermodynamically unstable with any organic solvent and the two react instantaneously to form an SEI. This SEI layer will continuously break down and regrow during Li deposition/stripping processes and is critical to the real growth pattern of reactive metals such as Li. Unfortunately, most models in the literature do not consider the impact of the SEI on the Li dendrite growth mechanisms. Recently, Cheng et al. (Cheng et al. 2015) reviewed the mechanisms of SEI formation and models of SEI structure. The critical factors affecting the SEI formation, such as electrolyte component, temperature, current density, are discussed. An extensive experimental study by Steiger et al. utilizing in situ light microscopy and ex situ SEM analysis concluded, however, that growth of the whisker/needle-like structures (often termed “dendrites”) occurs as follows (Steiger et al. 2014b, 2015; Steiger 2015):

- Li needle growth is generally initiated at either the substrate surface or from faceted particles of Li.
- Typically, the needles grow in length, but not in breadth.
- Growth often does not actually occur at the tip, but rather behind an inactive deposit located at the tip (possibly a particle of metal oxide, LiF or other SEI components) (Figs. 2.13, 2.14) (Steiger et al. 2014a).
- Li^+ cation transport through a thin SEI layer results in the overall needle growth which occurs—as just noted—at the needle tip (i.e., deposit-Li interface), at the base (i.e., substrate-Li interface), and at defects resulting in kinks in the needles.
- Extensive shaking/twisting motions transpire during the needle growth process (Steiger et al. 2014a; Brissot et al. 1998; Nishikawa et al. 2007, 2010, 2011, 2012; Nishida et al. 2013; Yamaki et al. 1998)—a characteristic that is readily explained by the differing growth zones (kinks and interfaces) in Steiger’s model.

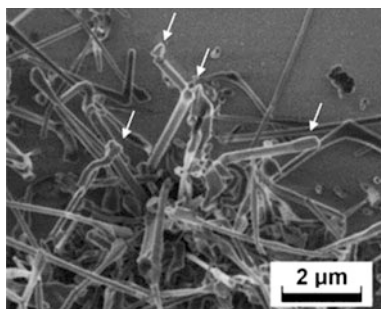


Fig. 2.13 SEM image of Li needle deposits on W (*arrows point to broadening and/or particles at tips*). Reproduced with permission—Copyright 2014, Elsevier (Steiger 2015)

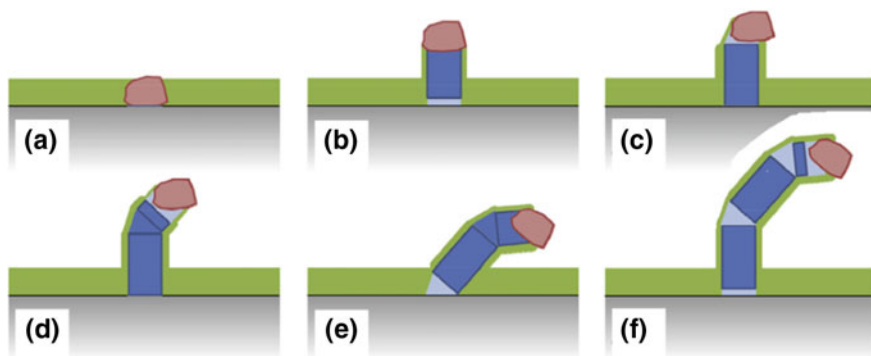


Fig. 2.14 Schematic describing growth of a Li needle: (*green*) SEI—probably mainly organic; (*light blue*) Li insertion areas and (*red*) inert tip. **a** Initial state before Li deposition with an inert inhomogeneity within the SEI, **b** after growing a straight segment by Li insertion at the substrate, **c** after further deposition taking place below the tip, **d** further deposition resulting in a kink, **e** additional Li inserted at the base, causing tilting motions of the whole structure and **f** final structure. All steps proceed by Li insertion into the growing structure. Reproduced with permission—Copyright 2014, Elsevier (Steiger et al. 2014a)

A number of these points were also previously emphasized in publications by Yamaki et al. (1998) and Nishikawa et al. (2011). Note that Steiger’s model—which explains the observed Li kinked whisker/needle-like growth patterns quite well—diverges significantly from previous models that have emphasized dendrite formation due to the depletion of Li^+ cations near the electrode surface, field enhancement at the needle (“dendrite”) tips, the strong influence of concentration gradients, and stresses that induce needle motion. Figure 2.15 shows SEM images of Li deposits on a stainless steel (SS) electrode after different times during which the electrode was polarized to -150 mV (versus Li/Li^+) in 1 M LiPF_6 -EC/DMC electrolyte and 1 M N_{1114} TFSI-LiTFSI (IL-based) electrolytes (Stark et al. 2013).

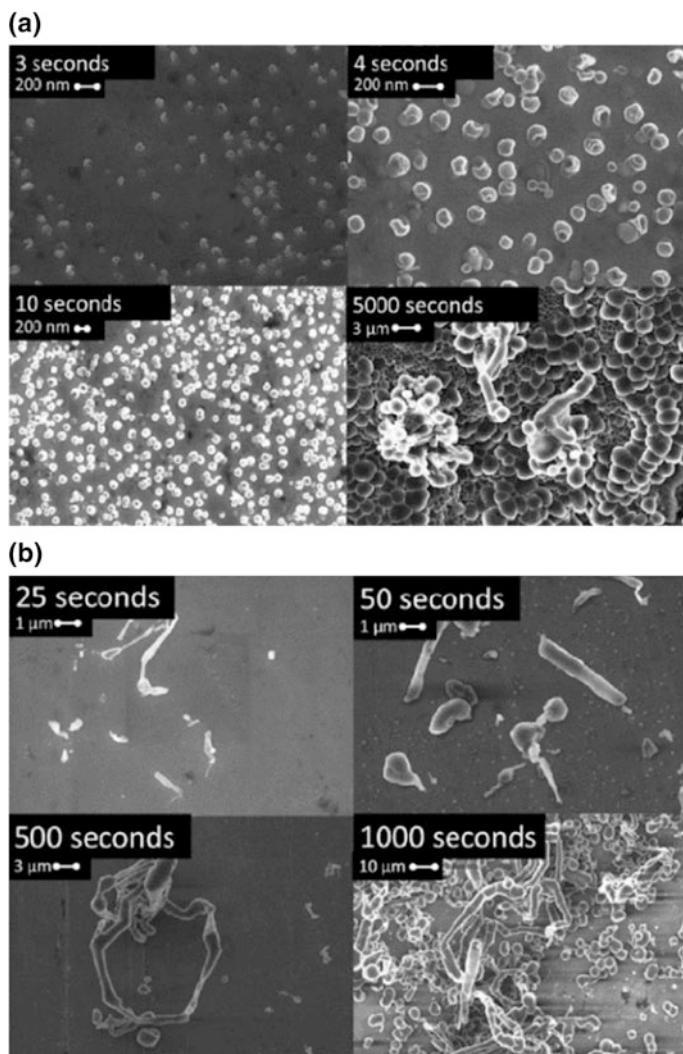


Fig. 2.15 SEM images of Li deposits on a SS electrode after the indicated plating times during which the electrode was polarized to -150 mV (versus Li/Li^+) in **a** 1 M LiPF_6 -EC/DMC electrolyte and **b** 1 M N_{1114} TFSI-LiTFSI (IL-based) electrolytes. Reproduced with permission—Copyright 2013, The Electrochemical Society (Stark et al. 2013)

When the Li deposition rate is slow, the Li nuclei formed initially will merge together as shown in Fig. 2.15a. When the needles grow fast relative to the nucleation points, then tangled fibrous aggregates of the kinked needles tend to result (Fig. 2.15b).

Very different Li deposition is sometimes observed that is referred to as non-dendritic—i.e., the Li has a particulate/nodular structure, which may be fused into

aggregated lumps or instead simply clustered together. This then requires a growth model that diverges from the linear needle model noted above. The Li deposition morphology is governed by Li^+ cation mobility, Li^0 (adatom) transport on the Li surface, and perhaps to some extent Li^0 self-diffusion within the bulk of the Li. Most of the focus in many mathematical models developed is on the former (i.e., Li^+ cation mobility within the electrolyte). Jäckle and Groß found that Li^0 atom self-diffusion has relatively high barriers on the most energetically favorable surfaces of the Li body-centered cubic (bcc) crystal and also has a lower tendency (than Mg, for example) to adopt high-coordination configurations (Jäckle and Groß 2014). This reduces the driving force for surface reconstruction from needle-like to nodular shapes. Higher temperatures—with the corresponding increase in Li^0 adatom mobility—would therefore be expected to favor more nodular Li structures (Aryanfar et al. 2015) and this will be shown below to indeed be the case. Another important consideration, however, is the Li^+ cation transport rate through the SEI to the Li growth surface. As noted above, the kinked needle growth may be dictated by favorable insertion of Li^0 adatoms at the tip (often below an inactive particle), the base and at defects resulting in one-dimensional growth. These may be locations where the resistance is lowest to Li^+ cation transport through the SEI or alternatively locations which have the lowest interfacial energy and thus serve as a sink for the adatoms. Transport, however, will be more favorable throughout the entire SEI layer at higher temperature and/or for a more conductive/thinner SEI. Thus, temperature and electrolyte composition strongly impact the Li deposition morphology (Nishikawa et al. 2011).

It will be shown below that such growth actually begins as needles which then thicken into nodules—that is, the one-dimensional, linear elongation which creates the needles transitions at some point to three-dimensional growth at the needle tips and defects or alternatively thickening of the entire needle segment(s) (Steiger et al. 2014b; Steiger 2015; Arakawa et al. 1993; Nishikawa et al. 2011, 2012). A highly aligned Li growth pattern was observed when a robust and uniform SEI layer formed on the surface of the substrate as reported recently by Qian et al. (2015a), i.e., the one-dimensional, linear elongation that creates the needles transitions at some point to three-dimensional growth.

The trace amount of HF derived from the decomposition reaction of LiPF_6 with H_2O is electrochemically reduced during the initial Li deposition process to form a uniform and dense LiF-rich SEI layer on the surface of the substrate. This SEI layer is robust and leads to a uniform distribution of the electric field on the substrate surface. In case of low rate deposition, the merged Li particles will favor growth into linear arrays of closely packed nanorods, since neighboring nanorods constrain the formation of the kinked defects, thereby enabling uniform and dendrite-free Li deposition. The surface and cross-section images of the as-deposited, dendrite-free Li films exhibit a self-aligned and highly compact Li nanorod structure as shown in Fig. 2.16, which is consistent with a vivid blue color due to structural coloration. Similar surface morphology was also observed before by several other groups (Stark et al. 2013; Zhang et al. 2014; Qian et al. 2015a).

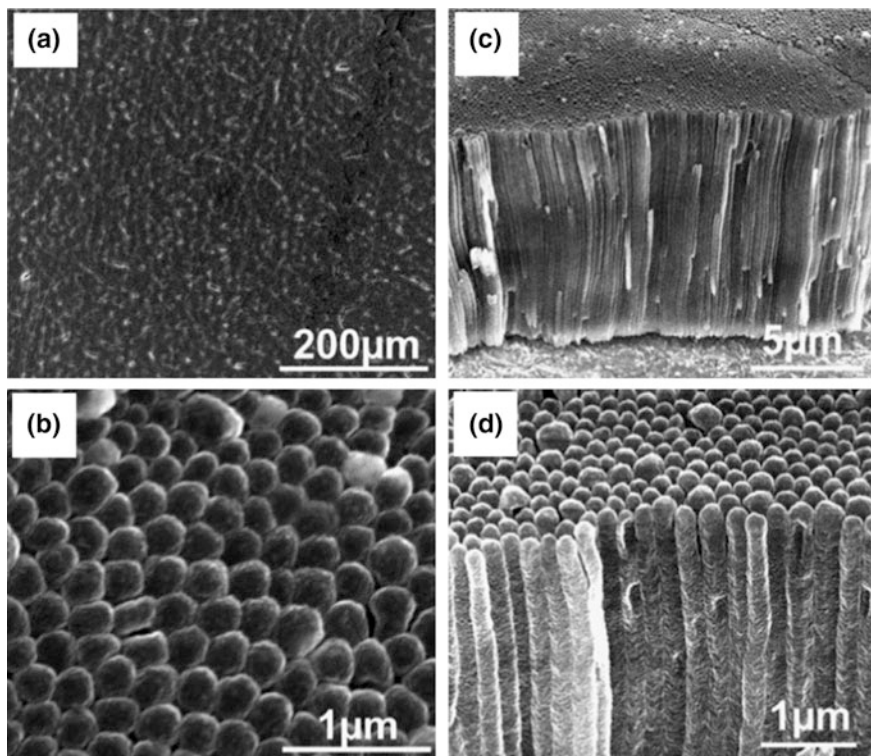


Fig. 2.16 SEM images of the morphologies of Li plated in a 1 M LiPF_6 -PC electrolyte with 50 ppm H_2O additive: **a, b** surface images and **c, d** cross-sectional images. Reproduced with permission—Copyright 2015, Elsevier (Qian et al. 2015a)

2.2.1 “Dead” Lithium

In an early publication in 1974, the effect of aging on the cycling CE of electrodeposited Li was examined using a 1 M LiClO_4 -PC electrolyte (Selim and Bro 1974). It was noted that the Li was mossy in appearance and that the CE (i.e., stripping/deposition charge ratio) decreased much more rapidly with increasing age of the deposit than did the Li metal content of the deposit (as determined chemically by reacting the Li with water and monitoring the amount of evolved gas generated). For example, after 40 h the CE approached zero, while the chemical analysis indicated that 80 % of the deposited Li remained (but could not be stripped from the electrode). This electrochemically unrecoverable Li has come to be known as “dead” Li (Yoshimatsu et al. 1988; Arakawa et al. 1993; Steiger et al. 2014b). Steiger et al. proposed a mechanism for this that illustrates how the “dead” Li may remain in physical, but not electrical contact with the electrode surface (Fig. 2.17) (Steiger et al. 2014b). This explains why after stripping the electroactive Li from a

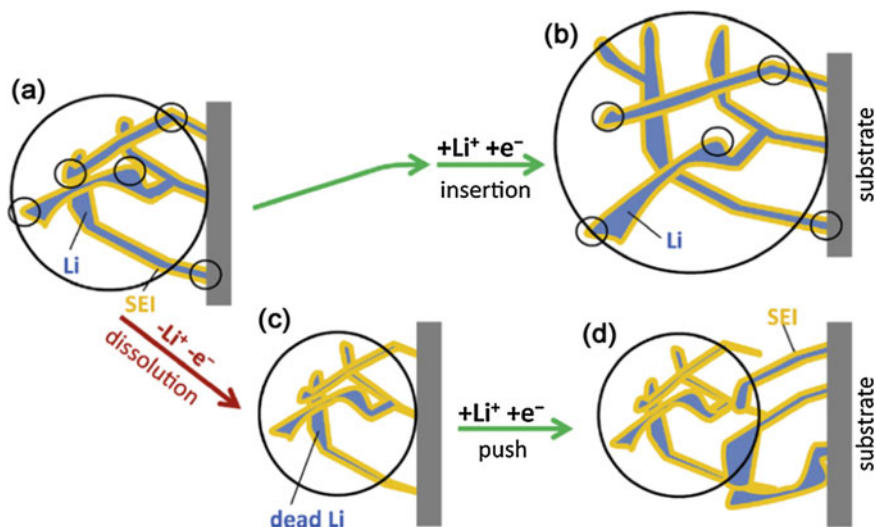


Fig. 2.17 Schematic of proposed growth mechanism for mossy Li. The structure is always covered by an SEI layer: **a** as-deposited, **b** the structure of (a) after further electrodeposition. Li atoms are inserted into the metal structure. Points have been marked with black circles to illustrate that the distances between these features generally increase with Li deposition time. The large black oval shape indicates the expansion of the total structure. **c** The structure of (a) after a dissolution step. The tips of the structure still contain Li metal (“dead” Li), but are electrically isolated from the substrate, although still being held by the former SEI shell. **d** Structure of (c) after an additional electrodeposition step. The top is pushed outward by the new mossy Li growing underneath. Reproduced with permission—Copyright 2014, Elsevier (Steiger et al. 2014b)

previous electrodeposition, new needle-like Li deposits often tend to grow on the electrode surface instead of on the previous (residual) material on the electrode surface (Brissot et al. 1998). This continues until the entire surface of the electrode is covered by the needles and their SEI residue. Thus, the interphasial layer on the surface of the Li may actually grow/accumulate predominantly at the working electrode surface rather than at the interphasial layer/electrolyte interface.

It has been reported from in situ visualization studies for both liquid and polymer electrolytes that dendrites are often not evident during the first few cycles at higher current densities (for which the CE is often relatively high), but then dendrites form and grow in subsequent cycles (often resulting in a continuous decline in the CE with continued cycling) (Dampier and Brummer 1977; Brissot et al. 1998, 1999b). This may be explained by the growth of short new needle-like deposits on the electrode surface during the first few cycles until the electrode is covered in its entirety by the SEI residue and “dead” Li. Then, breakaway Li dendritic structures form while Li deposits on the electrode escape in the following cycles through defects in this resistive layer, culminating in the exposure of protruding kinked needles for which Li^0 adatom addition is more facile, thus resulting in rapid growth of such dendrites.

2.2.2 Interphasial Layer and Formation of Mossy Lithium

For Li-ion batteries in which graphite is used as the anode, the SEI is generally a thin layer of reaction products formed from the degradation of the graphite (near the electrolyte interface), Li, solvent molecules, anions and/or other electrolyte components. Comparable SEI layers may form on the Li metal surface as noted in the discussion above on the needle growth mechanism. But rather than passivating the electrode from further reactions with the electrolyte, the dead Li forms an interphasial porous degradation layer (often termed “mossy” Li) that is much more substantive than the relatively thin SEI layer formed on the graphite surface. Upon cycling, there is thus a transition from a flat, smooth morphology to a rugged structure with a surface interphasial layer that continues to grow in thickness upon cycling (Figs. 2.18, 2.19) (Naoi et al. 1996; Orsini et al. 1998, 1999; López et al. 2009, 2012; Chang et al. 2015; Lv et al. 2015). In comparison, more mossy Li is formed at low current density and more dendrite is formed at high-current density (Orsini et al. 1999). The increased resistance results in increased polarization (i.e., higher absolute voltages for plating/stripping) (Fig. 2.20) and the “dead” Li may mask portions of the electrode (i.e., reduce the active surface area available for

Fig. 2.18 Sectioned Li battery after charging (0.45 mA cm^{-2}): **a** first charge and **b** 14th charge. Reproduced with permission —Copyright 1998, Elsevier (Orsini et al. 1998)

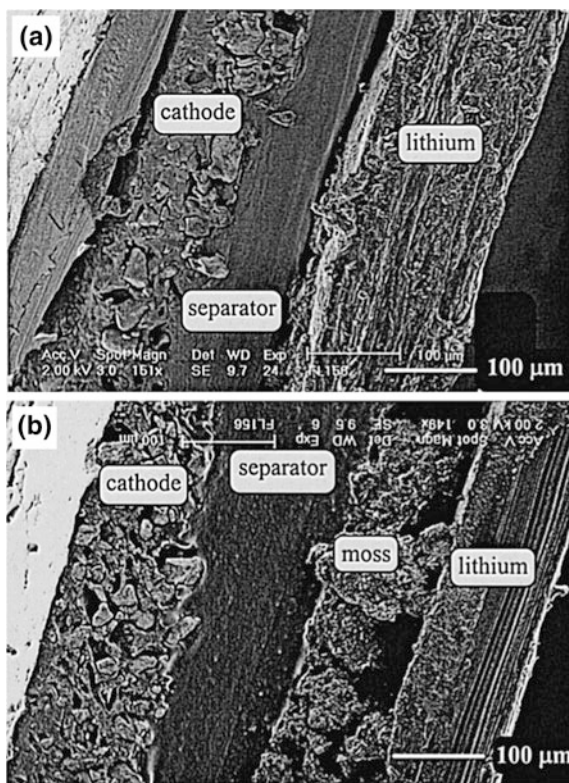
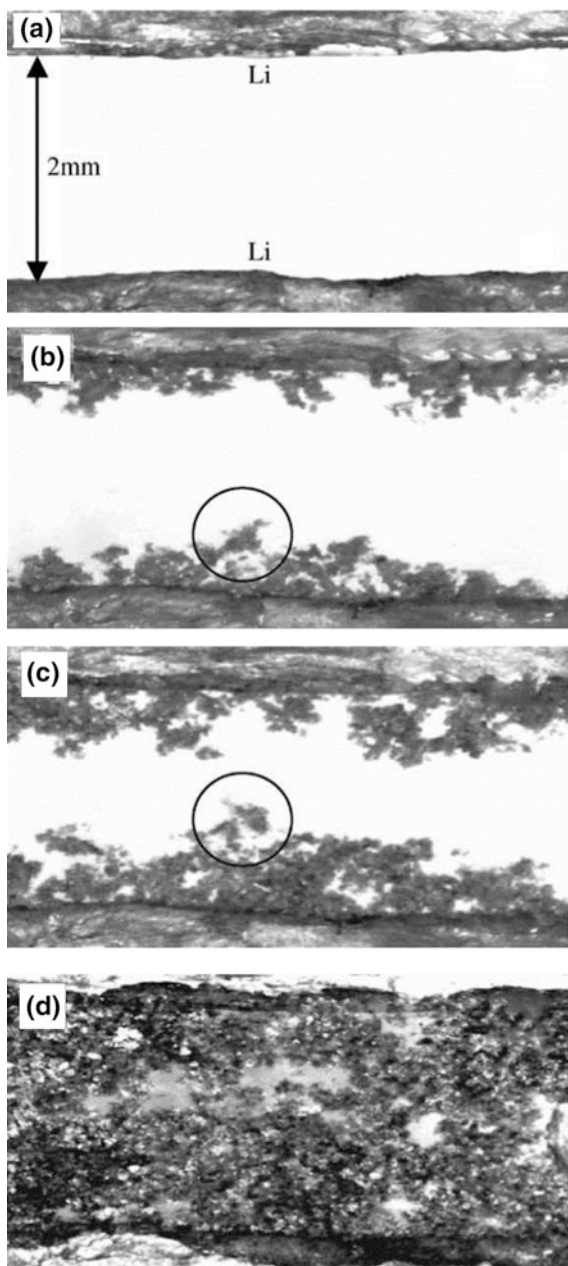


Fig. 2.19 Morphological changes during cycling between two Li electrodes in a 1 M LiPF₆-PC electrolyte at a current density of 1 mA cm⁻²; **a** uncycled, **b** 100 cycles, **c** 200 cycles and **d** 500 cycles. Reproduced with permission—Copyright 2003, Elsevier (Howlett et al. 2003)



deposition), thus increasing the effective current density which, as will be shown below, often results in more rapid Li consumption and possibly increased dendritic Li growth. This depletion of the electrolyte and electroactive Li due to degradation

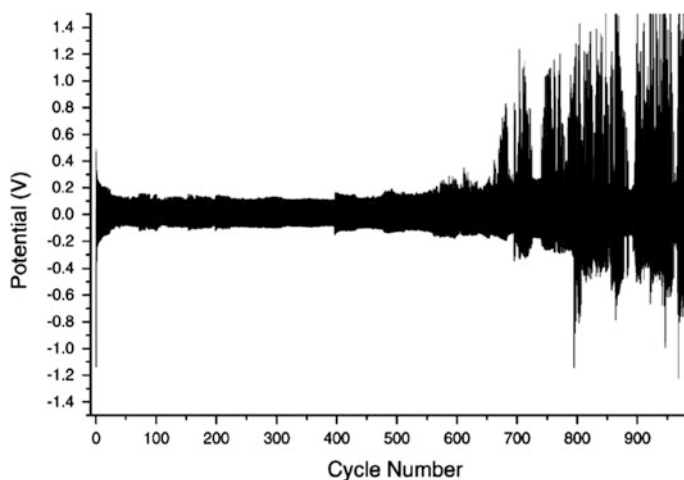


Fig. 2.20 Voltage profile for a Li||Li cell with a 1 M LiPF₆-PC electrolyte cycled at a current density of 1 mA cm⁻². Voltage spikes are due to temporary short circuits. Reproduced with permission—Copyright 2003, Elsevier (Howlett et al. 2003)

reactions, as well as the increased interfacial resistance from the porous interphasial layer, has been delineated as a principal cause of cell performance degradation and failure (Fig. 2.21) (Lv et al. 2015), although dendritic short circuiting may occur in some instances (López et al. 2009, 2012; Orsini et al. 1998, 1999; Yoshimatsu et al. 1988). Thus, the large voltage spikes in Fig. 2.20 originate from the highly resistive interphase rather than from short circuiting (which would result in a very low potential between the electrodes). Importantly, for full batteries, the loss of electrolyte (and the corresponding significant impedance increase) may ultimately be the key factor for the deterioration of the cell capacity rather than formation of the interphasial layer (Aurbach et al. 2000).

2.3 Modeling of Lithium Dendrite Growth

Significant work has been done to simulate and predict the growth pattern of Li dendrite growth in the last half-century. When an electrochemical cell containing an electrolyte with a Li salt is sufficiently polarized, Li⁺ cations near the negative electrode are reduced to Li metal and—depending upon the applied current density and the electrolyte’s transport properties—the Li⁺ cation concentration decreases resulting in anion migration toward the positive electrode until equilibrium is reached. The newly formed Li metal may deposit as a relatively compact layer or in a variety of other morphologies which are often described as dendritic. A recent review of models for dendrite initiation/propagation described three classifications (Li et al. 2014b):

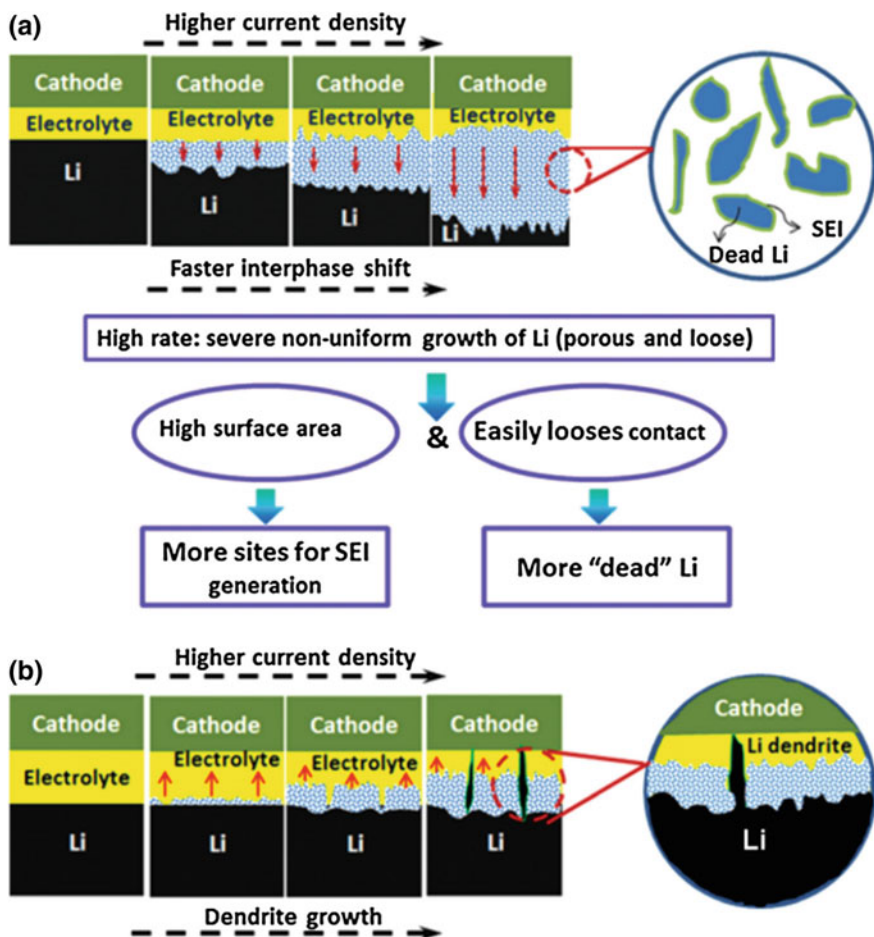


Fig. 2.21 Failure mechanism of the Li anode at high charge current densities: **a** schematic illustration of the failure mechanism and **b** conventional understanding of the dendrite-related failure mechanism for Li batteries. Reproduced with permission—Copyright 2014, Wiley-VCH (Lv et al. 2015)

1. Surface Tension Model—This model finds that electrodeposition is more rapid on projections rather than planar surfaces because spherical rather than linear diffusion dominates the mass transport of the active species. A larger spherical diffusion flux results in a narrowing of the growing dendrite tip; thus surface forces and mass transport dominate the kinetics governing dendrite growth (Monroe and Newman 2003, 2004, 2005; Barton and Bockris 1962; Diggle et al. 1969).
2. Brownian Statistical Simulation Model—This model focuses on the competition between ion transport and reductive deposition. When deposition probability is

low, Li^+ cation transport dominates and the ions penetrate close to the substrate resulting in a dense plating morphology with a low tendency for dendrite formation. This is contrasted with the case of high-deposition probability (relative to the cation transport), which increases the rate of deposition at the tip of projecting growth structures thus increasing the tendency for dendrite formation (Mayers et al. 2012; Voss and Tomkiewicz 1985; Magan et al. 2003).

3. Chazalviel Electromigration-Limited Model—This model for dendrite growth is often cited: at a time τ called the Sand time, the Li^+ cation concentration drops to zero at the negative electrode with high currents, causing the potential to diverge; this results in an instability at the interface from inhomogeneities in the distribution of the surface potential, which creates a localized electric field that leads to dendrite growth. The dendrite initiation time thus corresponds to the buildup of the space charge and the dendrite propagation velocity is tied to the transport of the anions (Brissot et al. 1998; Chazalviel 1990).

In addition to these, several new models have recently been proposed to describe Li plating/growth (Akolkar 2013, 2014; Chen et al. 2015; Cogswell 2015; Tang et al. 2009; Aryanfar et al. 2014). More details on a few of these important models of dendrite growth will be discussed in this section.

2.3.1 General Models

In the field of electrodeposition, metal “dendrites” are a common phenomenon. At a given electrodeposition condition, many metals, such as zinc (Zn), copper (Cu), silver (Ag), and tin (Sn), were reported to exhibit ramified morphologies (Chazalviel 1990). Fractal deposits including needle-like, snowflake-like, tree-like, bush-like, moss-like, and whisker-like structures are all referred to as dendrites in this review. Extensive work has been done on the dendrite formation mechanism during electrodeposition of Zn and Cu. Various strategies have been unitized to suppress dendrite growth in these processes (Sawada et al. 1986; Diggle et al. 1969). The reported methods to suppress Zn dendrites include special separators, alternating current or pulsed charging, and additives in the electrolytes. The last methods can be further divided into three categories: electrode structural modifiers, metallic additives, and organic additives (Lan et al. 2007). Several factors such as Zn concentration, complexing agents, anions, and additives may modify the texture and morphology of Zn electrodeposited coatings (Mendoza-Huizar et al. 2009). Recently, Aaboubi et al. (2011) investigated the effect of tartaric acid on Zn electrodeposition from a sulfate plating bath by electrochemical impedance spectroscopy (EIS), stationary polarization curves, XRD, and SEM imagery. The study shows that it is possible to obtain homogeneous, compact, and dendrite-free Zn deposits from sulfate solutions containing tartaric acid. Miyazaki et al. (2012)

also reported suppression of dendrite formation in metallic Zn deposition using zinc oxide electrodes modified with an anion-exchange ionomer (AEI). These improvements are explained by selective ion permeation through the AEI films. These approaches on Zn dendrite suppression and the techniques used in the investigation of Zn dendrite suppression and the techniques used in the investigation of Zn dendrite growth are very useful for the investigation and prevention of Li dendrite growth.

Although most electrodepositions are a one-time-only process, in a rechargeable Li metal battery, Li metal needs to be plated on or stripped from substrates repeatedly during charge/discharge processes. As a result, Li dendrites will accumulate on the anode and finally lead to many serious problems (see Fig. 1.1) that hamper the practical application of rechargeable Li metal batteries. Therefore, a good understanding of the mechanism of Li dendrite formation and growth is critical to mitigate or further eliminate Li dendrites.

Many groups have simulated the Li dendrite formation and growth process, and proposed several meaningful and fundamental models in the last forty years. In order to simplify the simulation conditions, most models were based on a binary electrolyte with a Li salt and polymer; for example, LiClO_4 or $\text{LiN}(\text{SO}_2\text{CF}_3)_2$ (LiTFSI) in polyethylene oxide (PEO). In the open circuit condition, the electrolyte is in a steady state without an ionic concentration gradient; under polarization, the Li^+ and anion will diverge and transfer to the negative and positive electrode, respectively. Li^+ will obtain an electron and plate on the negative electrode. The speed of Li deposition or consumption of Li^+ depends on the applied current density. Although the depletion of Li^+ can be macroscopically compensated by the supply of Li^+ from the positive electrode, the microscopic ionic distribution near the negative electrode dramatically affects the deposit's morphology. Therefore, a basic model to simulate Li dendrite starts from the calculation of the concentration gradient in the Li symmetric cell under polarization. Brissot and Chazalviel et al. described the concentration gradient in a cell with a small inter-electrode distance using the following equation (Rosso et al. 2006; Brissot et al. 1999b):

$$\frac{\partial C}{\partial x}(x) = \frac{J\mu_a}{eD(\mu_a + \mu_{\text{Li}^+})} \quad (2.1)$$

where J is the effective electrode current density, D is the ambipolar diffusion coefficient, e is the electronic charge, and μ_a and μ_{Li^+} are the anionic and Li^+ mobilities. From Eq. (2.1), two different conditions for a symmetrical Li/PEO/Li cell can be anticipated, with the inter-electrode distance L and initial Li salt concentration C_0 :

- (a) If $dC/dx < 2C_0/L$, the ionic concentration evolves to a steady state where the concentration gradient is constant and varies almost linearly from $C_a = C_0 - \Delta C_a$ at the negative electrode to $C_{\text{Li}^+} = C_0 + \Delta C_{\text{Li}^+}$ at the positive electrode, where

$$-\Delta C_a \approx -\Delta C_{Li^+} \approx \frac{\mu_a}{\mu_a + \mu_{Li^+}} \frac{JL}{eD} \quad (2.2)$$

- (b) If $dC/dx > 2C_0/L$, the ionic concentration goes to zero at the negative electrode at a time called “Sand’s time” τ , which varies as

$$\tau = \pi D \left(\frac{eC_0}{2Jt_a} \right)^2 \quad (2.3)$$

$$t_a \approx 1 - t_{Li^+} = \frac{\mu_a}{\mu_a + \mu_{Li^+}} \quad (2.4)$$

where t_a and t_{Li^+} represent the anionic and Li^+ transference number, respectively. Chazalviel indicated that the anionic and Li^+ concentrations exhibit different behaviors at the Sand time, leading to an excess of positive charge at the negative electrode. This behavior will result in a local space charge, form a large electric field, and lead to nucleation and growth of Li dendrite. The results of their simulations and experiments confirmed the concentration gradient and the occurrence of dendrites very close to Sand’s time (Brissot et al. 1998, 1999a). Chazalviel (1990) also predicted that the dendrite will grow at the velocity of

$$v = -\mu_a E \quad (2.5)$$

where E is the electric field strength.

Monroe and Newman developed the general model describing dendrite growth under galvanostatic conditions applicable to liquid electrolytes (Monroe and Newman 2003). They adopted the Barton and Bockris method (Barton and Bockris 1962) with the addition of thermodynamic reference points and the fact that concentration and potential are not constant during the course of dendrite growth. They calculated the concentration and potential distribution in the cell at different time intervals. It was demonstrated that the dendrite growth rate increases across the electrolyte and depends greatly on the applied current density; this will be discussed in more detail in the following section.

Rosso et al. reported a systematic study on the evolution of Li dendrites in LiTFSI-PEO electrolyte involving theoretical calculations as well as experimental data (Rosso et al. 2006). They demonstrated that even though the formation of dendrites has little effect on overall impedance, it significantly decreases interfacial impedance. Based on the impedance data, the value of resistance due to the dendrites could be calculated. In addition, it was observed that dendrites can burn out like a fuse; that is, when the first dendrite reaches the opposite electrode it shorts the circuit and the current density passing through this single dendrite becomes high enough to melt it. Thus, the final short circuit occurs only when the major front of dendrites eventually reaches the opposite electrode.

Although the formation of contiguous and conducting Li dendrites in batteries is often called “dendritic growth,” there are actually several modes of formation and growth: dendrites, whiskers, and “others.” The true dendrite grows from a Li metal surface in a nonaqueous electrolyte by adding material to its tip. The nutrient source is the Li in the electrolyte. Classical models of dendrite growth gave solutions in the form of the tip radius times its velocity, which has the units of diffusivity. Recent electrochemical continuum models (Rosso et al. 2001) and experiments (Bhattacharyya et al. 2010) for Li batteries have found that the dendrite growth is controlled by the tip surface energy, always accelerates across the cell under all conditions, and can be partially mitigated by lowering the limiting current or increasing the cell thickness. The latter two conditions limit the performance of the battery. A second type of growth has been simulated in some Li battery experiments. If the nutrient supply is drawn from the Li metal sheet, growth occurs at the base of a “whisker.” Yamaki (1998) analyzed the stress-assisted whisker growth through cracks in a protective layer (i.e., the separator) on the surface of the Li anode.

2.3.2 Effect of Current Density

It is well known that the effective current density during Li deposition/stripping has a significant impact on the dendrite formation and growth. Generally, low current density results in relatively stable cycling, and conversely, high current density accelerates the degradation process of rechargeable Li metal batteries. The equation of Sand’s time indicates that the dendrite initiation time is proportional to J^{-2} , which indicates that high current density greatly accelerates the formation of Li dendrites. It is worth noting that there are some results showing $\tau \sim J^{-1.25}$ rather than $\tau \sim J^{-2}$ dependence, as reported by (Liu et al. 2010). They attributed this deviation to the local fluctuations of current density. Moreover, the ionic liquid (IL) used in their work acted as a supporting electrolyte. In fact, this is a ternary electrolyte rather than a binary one as assumed by Chazalviel’s model. In the model developed by Monroe and Newman (2003) using liquid electrolyte, tip growth rate (v_{tip}) can be expressed as

$$v_{\text{tip}} = \frac{J_n V}{F} \quad (2.6)$$

where J_n is the effective current density normal to the dendrite (hemispherical) tip, V is the molar volume of Li and F is Faraday’s constant. This equation suggests that the dendrite growth rate is proportional to J_n . Based on Eq. (2.3) and (2.6), the dendrite initiation time could be delayed and the dendrite growth rate could be slowed down if the effective current density could be decreased. By applying a smaller current density, a smoother surface and improved cycling life have been

obtained (Kanamura et al. 1996; Aurbach et al. 2000; Zinigrad et al. 2001; Wang et al. 2000; Crowther and West 2008; Gireaud et al. 2006).

According to Chazalviel's model, an applied current density leads to an ion concentration gradient—high-current density results in near-zero ion concentration at the negative electrode and the formation of Li dendrites at Sand's time, low current density leads to a minimal and stable ion concentration gradient so no Li dendrites form in this condition. The crossover between the two regimes is the limiting current density

$$J^* = 2eC_0D/t_aL \quad (2.7)$$

where L is the inter-electrode distance, t_a is the anionic transport number. When the current density is low or the inter-electrode distance L is small, there is in principle no Sand behavior and the concentration variation should be small. However, experimental results clearly indicate there are still Li dendrites, just not as serious as those at high-current density. Rosso et al. (2001) and Teyssot et al. (2005) attributed the formation of dendrites to local nonuniformity of the Li/electrolyte interface, which leads to a large concentration variance even in the depleted zone close to the conditions of Chazalviel's model. Brissot et al. (1998) confirmed this experimentally in a Li|LiTFSI-PEO|Li cell although individual dendrites could deviate from the predicted growth rate. It was demonstrated that at high current densities (when Li deposition becomes diffusion controlled), the onset of dendrite formation matched Sand's time (zero ion concentration). However, dendrites started to grow earlier with cycling, apparently because of the created defects. At low current densities (i.e., when concentration variations were low), dendrites were also observed in the form of elongated metal filaments (higher aspect ratio), which could be a result of local inhomogeneity. Growth velocities followed Chazalviel's model (Chazalviel 1990) in both cases. It was later shown by Rosso et al. (2001) that the time of dendrite appearance at low current densities is also proportional to the power of current density even though Sand's behavior was not expected. It was proposed that the specific properties of LiTFSI-PEO electrolyte cause destabilization of the concentration distribution along the electrode surface. A direct relation between dendritic growth and concentration gradient was clearly demonstrated by employing three independent techniques to measure ion concentrations in the vicinity of dendrites (Brissot et al. 1999a).

In addition to the value of current density, the charging styles, galvanostat, or pulse also significantly affects Li dendrite formation and growth. Recent work by Miller and coauthors reported that pulsed charging can effectively suppress Li dendrite formation by as much as 96 %. They proposed a coarse-grained lattice model to explain the mechanism of pulsed charging and revealed that dendrite formation arose from a competition between the time scales of Li^+ diffusion and reduction at the anode, with lower overpotential and shorter electrode pulse durations shifting this competition in favor of lower dendrite formation probability (Mayers et al. 2012).

2.3.3 Importance of Interfacial Elastic Strength

Monroe and Newman (2005) further employed linear elasticity theory to develop a kinetic model describing how mechanical properties of polymer electrolytes (shear modulus and Poisson's ratio) affect roughness on the Li interface. The interface was subjected to a regime of small-amplitude two-dimensional (2D) perturbations. Analytic solutions with specific boundary conditions allowed computing deformation profiles. Compressive stress, deformation stress, and surface tension at the elastic Li interface were calculated as a next step. Incorporation of these parameters into the model gave a prediction of the distribution of exchange current density along the electrode surface. Finally, it was possible to verify that the mechanical properties of the polymer electrolyte stopped amplification of the dendrite growth. It turned out that dendrite suppression can be achieved when the shear modulus of the electrolyte is about twice that of the Li anode ($\sim 10^9$ Pa); that is, at least three orders of magnitude higher than that of the studied PEO.

As in many other fields, all of the models discussed above have their limitations. For example, the dendrite growth velocity proposed by Monroe and Newman (2003) (Eq. (2.6)) was derived from the growth of a single dendrite without considering the interaction between neighboring dendrites. It was also stated that the Chazalviel theory (Chazalviel 1990) has limited application in real batteries because it applies at currents higher than the limiting current. However, Rosso et al. (2001) and Teyssot et al. (2005) concluded that the Chazalviel model can be extended to low currents due to the nanoscale inhomogeneity in concentration, at least in the case of PEO-based electrolytes. Even though these models still include many simplifications and limitations, they have established a solid foundation for the nucleation and growth mechanisms of dendrites. More importantly, as we will discuss later in this book, several general predications of these models have been used successfully to identify new approaches to suppress dendrite growth, especially during Li metal deposition; for example, using an anode with large surface area to reduce the effective current density, developing a single ion conductor to enhance Li^+ transference number, developing an electrolyte with strong shear modulus, and adding supporting electrolyte. These approaches will be discussed in detail in Chap. 3.

References

- Aaboubi O, Douglade J, Abenagui X, Boumedmed R, VonHoff J (2011) Influence of tartaric acid on zinc electrodeposition from sulphate bath. *Electrochim Acta* 56(23):7885–7889
- Akolkar R (2013) Mathematical model of the dendritic growth during lithium electrodeposition. *J Power Sources* 232:23–28. doi:[10.1016/j.jpowsour.2013.01.014](https://doi.org/10.1016/j.jpowsour.2013.01.014)
- Akolkar R (2014) Modeling dendrite growth during lithium electrodeposition at sub-ambient temperature. *J Power Sources* 246:84–89. doi:[10.1016/j.jpowsour.2013.07.056](https://doi.org/10.1016/j.jpowsour.2013.07.056)

- Arai J, Okada Y, Sugiyama T, Izuka M, Gotoh K, Takeda K (2015) In situ solid state ^7Li NMR observations of lithium metal deposition during overcharge in lithium ion batteries. *J Electrochem Soc* 162(6):A952–A958. doi:[10.1149/2.0411506jes](https://doi.org/10.1149/2.0411506jes)
- Arakawa M, Tobishima S-I, Nemoto Y, Ichimura M (1993) Lithium electrode cycleability and morphology dependence on current density. *J Power Sources* 43–44:27–35
- Aryanfar A, Brooks D, Merinov BV, Goddard WA III, Colussi AJ, Hoffmann MR (2014) Dynamics of lithium dendrite growth and inhibition: pulse charging experiments and monte carlo calculations. *J Phys Chem Lett* 5(10):1721–1726. doi:[10.1021/jz500207a](https://doi.org/10.1021/jz500207a)
- Aryanfar A, Brooks DJ, Colussi AJ, Merinov BV, Goddard WA III, Hoffmann MR (2015) Thermal relaxation of lithium dendrites. *Phys Chem Chem Phys* 17(12):8000–8005. doi:[10.1039/c4cp05786d](https://doi.org/10.1039/c4cp05786d)
- Aurbach D, Cohen Y (1996) The application of atomic force microscopy for the study of Li deposition processes. *J Electrochem Soc* 143(11):3525–3532
- Aurbach D, Cohen Y (1997) Morphological studies of Li deposition processes in LiAsF_6/PC solutions by in situ atomic force microscopy. *J Electrochem Soc* 144(10):3355–3360
- Aurbach D, Daroux ML, Faguy PW, Yeager E (1987) Identification of surface films formed on lithium in propylene carbonate solutions. *J Electrochem Soc* 134(7):1611–1620
- Aurbach D, Gofer Y, Langzam J (1989) The correlation between surface chemistry, surface morphology, and cycling efficiency of lithium electrodes in a few polar aprotic systems. *J Electrochem Soc* 136(11):3198–3205
- Aurbach D, Youngman O, Dan P (1990a) The electrochemical behavior of 1,3-Dioxolane- LiClO_4 solutions—II. Contaminated solutions. *Electrochim Acta* 35(3):639–655
- Aurbach D, Youngman O, Gofer Y, Meitav A (1990b) The electrochemical behavior of 1,3-Dioxolane- LiClO_4 solutions—I. Uncontaminated Solutions. *Electrochim Acta* 35(3):625–638
- Aurbach D, Daroux M, McDougall G, Yeager EB (1993) Spectroscopic studies of lithium in an ultrahigh vacuum system. *J Electroanal Chem* 358:63–76. doi:[10.1016/0022-0728\(93\)80431-G](https://doi.org/10.1016/0022-0728(93)80431-G)
- Aurbach D, Weissman I, Zaban A, Chusid O (1994) Correlation between surface chemistry, morphology, cycling efficiency and interfacial properties of Li electrodes in solutions containing different Li salts. *Electrochim Acta* 39:51–71
- Aurbach D, Zaban A, Gofer Y, Ely YE, Weissman I, Chusid O, Abramson O (1995) Recent studies of the lithium-liquid electrolyte interface. electrochemical, morphological and spectral studies of a few important systems. *J Power Sources* 54:76–84
- Aurbach D, Zaban A, Ein-Eli Y, Weissman I, Chusid O, Markovsky B, Levi M, Levi E, Schechter A, Granot E (1997) Recent studies on the correlation between surface chemistry, morphology, three-dimensional structures and performance of Li and Li-C intercalation anodes in several important electrolyte systems. *J Power Sources* 68:91–98
- Aurbach D, Weissman I, Yamin H, Elster E (1998) The correlation between charge/discharge rates and morphology, surface chemistry, and performance of Li electrodes and the connection to cycle life of practical batteries. *J Electrochem Soc* 145(5):1421–1426
- Aurbach D, Markovsky B, Levi MD, Levi E, Schechter A, Moshkovich M, Cohen Y (1999) New insights into the interactions between electrode materials and electrolyte solutions for advanced nonaqueous batteries. *J Power Sources* 81–82:95–111
- Aurbach D, Zinigrad E, Teller H, Dan P (2000) Factors which limit the cycle life of rechargeable lithium (metal) batteries. *J Electrochem Soc* 147:1274–1279
- Barton JL, Bockris JOM (1962) The electrolytic growth of dendrites from ionic solutions. *Proc R Soc Lond A* 268:485–505
- Besenhard JO, Gürtler J, Komenda P, Paxinos A (1987) Corrosion protection of secondary lithium electrodes in organic electrolytes. *J Power Sources* 20:253–258
- Bhattacharyya R, Key B, Chen H, Best AS, Hollenkamp AF, Grey CP (2010) In situ NMR observation of the formation of metallic lithium microstructures in lithium batteries. *Nat Mater* 9(6):504–510. doi:[10.1038/nmat2764](https://doi.org/10.1038/nmat2764)

- Bieker G, Winter M, Bieker P (2015) Electrochemical in situ investigations of SEI and dendrite formation on the lithium metal anode. *Phys Chem Chem Phys* 17(14):8670–8679. doi:[10.1039/c4cp05865h](https://doi.org/10.1039/c4cp05865h)
- Brissot C, Rosso M, Chazalviel JN, Baudry P, Lascaud S (1998) In situ study of dendritic growth in lithium/PEO-salt/lithium cells. *Electrochim Acta* 43(10–11):1569–1574
- Brissot C, Rosso M, Chazalviel JN, Lascaud S (1999a) In situ concentration cartography in the neighborhood of dendrites growing in lithium/polymer-electrolyte/lithium cells. *J Electrochem Soc* 146(12):4393–4400
- Brissot C, Rosso M, Chazalviel JN, Lascaud S (1999b) Dendritic growth mechanisms in lithium/polymer cells. *J Power Sources* 81–82:925–929. doi:[10.1016/S0378-7753\(98\)00242-0](https://doi.org/10.1016/S0378-7753(98)00242-0)
- Chandrashekar S, Trease NM, Chang HJ, Du L-S, Grey CP, Jerschow A (2012) 7Li MRI of Li batteries reveals location of microstructural lithium. *Nat Mater* 11(4):311–315. doi:<http://www.nature.com/nmat/journal/v11/n4/abs/nmat3246.html#supplementary-information>
- Chang HJ, Trease NM, Ilott AJ, Zeng D, Du L-S, Jerschow A, Grey CP (2015) Investigating Li microstructure formation on Li anodes for lithium batteries by in situ 6Li/7Li NMR and SEM. *J Phys Chem C* 119(29):16443–16451. doi:[10.1021/acs.jpcc.5b03396](https://doi.org/10.1021/acs.jpcc.5b03396)
- Chazalviel JN (1990) Electrochemical aspects of the generation of ramified metallic electrodeposits. *Phys Rev A* 42(12):7355–7367. doi:[10.1103/PhysRevA.42.7355](https://doi.org/10.1103/PhysRevA.42.7355)
- Chen L, Zhang HW, Liang LY, Liu Z, Qi Y, Lu P, Chen J, Chen L-Q (2015) Modulation of dendritic patterns during electrodeposition: a nonlinear phase-field model. *J Power Sources* 300:376–385. doi:[10.1016/j.jpowsour.2015.09.055](https://doi.org/10.1016/j.jpowsour.2015.09.055)
- Cheng X-B, Zhang R, Zhao C-Z, Wei F, Zhang J-G, Zhang Q (2015) A review of solid electrolyte interphases on lithium metal anode. *Adv Sci*: 1500213
- Choi N-S, Koo B, Yeon J-T, Lee KT, Kim D-W (2011) Effect of a novel amphipathic ionic liquid on lithium deposition in gel polymer electrolytes. *Electrochim Acta* 56(21):7249–7255. doi:[10.1016/j.electacta.2011.06.058](https://doi.org/10.1016/j.electacta.2011.06.058)
- Cogswell DA (2015) Quantitative phase-field modeling of dendritic electrodeposition. *Phys Rev E* 92(1):011301. doi:[10.1103/PhysRevE.92.011301](https://doi.org/10.1103/PhysRevE.92.011301)
- Cohen YS, Cohen Y, Aurbach D (2000) Micromorphological studies of lithium electrodes in alkyl carbonate solutions using in situ atomic force microscopy. *J Phys Chem B* 104:12282–12291
- Crowther O, West AC (2008) Effect of electrolyte composition on lithium dendrite growth. *J Electrochem Soc* 155(11):A806–A811. doi:[10.1149/1.2969424](https://doi.org/10.1149/1.2969424)
- Dampier FW, Brummer SB (1977) The cycling behavior of the lithium electrode in LiAsF₆/methyl acetate solutions. *Electrochim Acta* 22:1339–1345
- Deng X, Hu MY, Wei X, Wang W, Chen Z, Liu J, Hu JZ (2015) Natural abundance ¹⁷O nuclear magnetic resonance and computational modeling studies of lithium based liquid. *J Power Sources* 285:146–155. doi:[10.1016/j.jpowsour.2015.03.091](https://doi.org/10.1016/j.jpowsour.2015.03.091)
- Dey AN (1976) S.E.M. studies of the Li-film growth and the voltage-delay phenomenon associated with the lithium-thionyl chloride inorganic electrolyte system. *Electrochim Acta* 21(5):377–382
- Diggle JW, Despic AR, Bockris JOM (1969) The mechanism of the dendritic electrocrystallization of zinc. *J Electrochem Soc* 112:1503–1514
- Ding F, Xu W, Graff GL, Zhang J, Sushko ML, Chen X, Shao Y, Engelhard MH, Nie Z, Xiao J, Liu X, Sushko PV, Liu J, Zhang J-G (2013) Dendrite-free lithium deposition via self-healing electrostatic shield mechanism. *J Am Chem Soc* 135(11):4450–4456. doi:[10.1021/ja312241y](https://doi.org/10.1021/ja312241y)
- Ding F, Xu W, Chen X, Zhang J, Shao Y, Engelhard MH, Zhang Y, Blake TA, Graff GL, Liu X, Zhang J-G (2014) Effects of cesium cations in lithium deposition via self-healing electrostatic shield mechanism. *J Phys Chem C* 118(8):4043–4049. doi:[10.1021/jp4127754](https://doi.org/10.1021/jp4127754)
- Dollé M, Sannier L, Beaudoin B, Trentin M, Tarascon J-M (2002) Live scanning electron microscope observations of dendritic growth in lithium/polymer cells. *Electrochem Solid-State Lett* 5(12):A286–A289. doi:[10.1149/1.1519970](https://doi.org/10.1149/1.1519970)
- Fujieda T, Yamamoto N, Saito K, Ishibashi T, Honjo M, Koike S, Wakabayashi N, Higuchi S (1994) Surface of lithium electrodes prepared in Ar + CO₂ Gas. *J Power Sources* 52:197–200. doi:[10.1016/0378-7753\(94\)01961-4](https://doi.org/10.1016/0378-7753(94)01961-4)

- Ghassemi H, Au M, Chen N, Heiden PA, Yassar RS (2011) Real-time observation of lithium fibers growth inside a nanoscale lithium-ion battery. *Appl Phys Lett* 99(12):123113. doi:[10.1063/1.3643035](https://doi.org/10.1063/1.3643035)
- Gireaud L, Grugeon S, Laruelle S, Yrieix B, Tarascon JM (2006) Lithium metal stripping/plating mechanisms studies: a metallurgical approach. *Electrochem Commun* 8(10):1639–1649. doi:[10.1016/j.elecom.2006.07.037](https://doi.org/10.1016/j.elecom.2006.07.037)
- Gu M, Parent LR, Mehdi BL, Unocic RR, McDowell MT, Sacci RL, Xu W, Connell JG, Xu P, Abellan P, Chen X, Zhang Y, Perea DE, Evans JE, Lauhon LJ, Zhang JG, Liu J, Browning ND, Cui Y, Arslan I, Wang CM (2013) Demonstration of an electrochemical liquid cell for operando transmission electron microscopy observation of the lithiation/delithiation behavior of Si nanowire battery anodes. *Nano Lett* 13(12):6106–6112. doi:[10.1021/nl403402q](https://doi.org/10.1021/nl403402q)
- Harry KJ, Hallinan DT, Parkinson DY, MacDowell AA, Balsara NP (2014) Detection of subsurface structures underneath dendrites formed on cycled lithium metal electrodes. *Nat Mater* 13(1):69–73. doi:[10.1038/nmat3793](https://doi.org/10.1038/nmat3793)
- Harry KJ, Liao X, Parkinson DY, Minor aM, Balsara NP (2015) Electrochemical Deposition and Stripping Behavior of Lithium Metal across a Rigid Block Copolymer Electrolyte Membrane. *J Electrochem Soc* 162(14):A2699–A2706
- Hernandez-Maya R, Rosas O, Saunders J, Castaneda H (2015) Dynamic characterization of dendrite deposition and growth in Li-surface by electrochemical impedance spectroscopy. *J Electrochem Soc* 162(4):A687–A696. doi:[10.1149/2.0561504jes](https://doi.org/10.1149/2.0561504jes)
- Howlett PC, MacFarlane DR, Hollenkamp AF (2003) A sealed optical cell for the study of lithium-electrode|electrolyte interfaces. *J Power Sources* 114(2):277–284. doi:[10.1016/s0378-7753\(02\)00603-1](https://doi.org/10.1016/s0378-7753(02)00603-1)
- Huang JY, Zhong L, Wang CM, Sullivan JP, Xu W, Zhang LQ, Mao SX, Hudak NS, Liu XH, Subramanian A, Fan H, Qi L, Kushima A, Li J (2010) In situ observation of the electrochemical lithiation of a single SnO₂ nanowire electrode. *Science* 330:1515–1520
- Ishikawa M, Morita M, Matsuda Y (1997) In situ scanning vibrating electrode technique for lithium metal anodes. *J Power Sources* 68:501–505
- Jäckle M, Groß A (2014) Microscopic properties of lithium, sodium, and magnesium battery anode materials related to possible dendrite growth. *J Chem Phys* 141(17):174710. doi:[10.1063/1.4901055](https://doi.org/10.1063/1.4901055)
- Kanamura K, Tamura H, Shiraishi S, Takehara Z-I (1995a) Morphology and chemical compositions of surface films of lithium deposited on a Ni substrate in nonaqueous electrolytes. *J Electroanal Chem* 394:49–62
- Kanamura K, Tamura H, Shiraishi S, Takehara Z-I (1995b) XPS analysis of lithium surfaces following immersion in various solvents containing LiBF₄. *J Electrochem Soc* 142(2):340–347
- Kanamura K, Shiraishi S, Takehara Z-I (1996) Electrochemical deposition of very smooth lithium using nonaqueous electrolytes containing HF. *J Electrochem Soc* 143(7):2187–2197
- Kanamura K, Takehara H, Shiraishi S, Takehara Z-I (1997) Chemical reaction of lithium surface during immersion in LiClO₄ or LiPF₆/DEC electrolyte. *J Electrochem Soc* 144(6):1900–1906
- Kominato A, Yasukawa E, Sato N, Ijuin T, Asahina H, Mori S (1997) Analysis of surface films on lithium in various organic electrolytes. *J Power Sources* 68:471–475
- Lan CJ, Lee CY, Chin TS (2007) Tetra-alkyl ammonium hydroxides as inhibitors of Zn dendrite in Zn-based secondary batteries. *Electrochim Acta* 52(17):5407–54116
- Lee Y-G, Kyhm K, Choi N-S, Ryu KS (2006) Submicroporous/microporous and compatible/incompatible multi-functional dual-layer polymer electrolytes and their interfacial characteristics with lithium metal anode. *J Power Sources* 163(1):264–268. doi:[10.1016/j.jpowsour.2006.05.008](https://doi.org/10.1016/j.jpowsour.2006.05.008)
- Lee YM, Seo JE, Lee Y-G, Lee SH, Cho KY, Park J-K (2007) Effects of triacetoxysilylsilane as SEI layer additive on electrochemical performance of lithium metal secondary battery. *Electrochem Solid-State Lett* 10(9):A216–A219. doi:[10.1149/1.2750439](https://doi.org/10.1149/1.2750439)
- Li W, Zheng H, Chu G, Luo F, Zheng J, Xiao D, Li X, Gu L, Li H, Wei X, Chen Q, Chen L (2014a) Effect of electrochemical dissolution and deposition order on lithium dendrite formation: a top view investigation. *Faraday Discuss* 176:109–124. doi:[10.1039/c4fd00124a](https://doi.org/10.1039/c4fd00124a)

- Li Z, Huang J, Liaw BY, Metzler V, Zhang J (2014b) A review of lithium deposition in lithium-ion and lithium metal secondary batteries. *J Power Sources* 254:168–182. doi:[10.1016/j.jpowsour.2013.12.099](https://doi.org/10.1016/j.jpowsour.2013.12.099)
- Liu S, Imanishi N, Zhang T, Hirano A, Takeda Y, Yamamoto O, Yang J (2010) Lithium dendrite formation in Li/Poly(ethylene oxide)–lithium Bis(trifluoromethanesulfonyl)imide and N-Methyl-N-propylpiperidinium Bis(trifluoromethanesulfonyl)imide/Li cells. *J Electrochem Soc* 157(10):A1092–A1098. doi:[10.1149/1.3473790](https://doi.org/10.1149/1.3473790)
- Liu XH, Zhong L, Zhang LQ, Kushima A, Mao SX, Li J, Ye ZZ, Sullivan JP, Huang JY (2011) Lithium fiber growth on the anode in a nanowire lithium ion battery during charging. *Appl Phys Lett* 98(18):183107. doi:[10.1063/1.3585655](https://doi.org/10.1063/1.3585655)
- López CM, Vaughey JT, Dees DW (2009) Morphological transitions on lithium metal anodes. *J Electrochem Soc* 156(9):A726–A729. doi:[10.1149/1.3158548](https://doi.org/10.1149/1.3158548)
- López CM, Vaughey JT, Dees DW (2012) Insights into the role of interphasial morphology on the electrochemical performance of lithium electrodes. *J Electrochem Soc* 159(6):A873–A886. doi:[10.1149/2.100206jes](https://doi.org/10.1149/2.100206jes)
- Lv D, Shao Y, Lozano T, Bennett WD, Graff GL, Polzin B, Zhang J-G, Engelhard MH, Saenz NT, Henderson WA, Bhattacharya P, Liu J, Xiao J (2015) Failure mechanism for fast-charged lithium metal batteries with liquid electrolytes. *Adv Energy Mater* 5(3):1400993. doi:[10.1002/aenm.201400993](https://doi.org/10.1002/aenm.201400993)
- Magan RV, Sureshkumar R, Lin B (2003) Influence of surface reaction rate on the size dispersion of interfacial nanostructures. *J Phys Chem B* 107:10513–10520
- Matsuda Y, Ishikawa M, Yoshitake S, Morita M (1995) Characterization of the lithium-organic electrolyte interface containing inorganic and organic additives by in situ techniques. *J Power Sources* 54:301–305
- Mayers MZ, Kaminski JW, Miller TF (2012) Suppression of dendrite formation via pulse charging in rechargeable lithium metal batteries. *J Phys Chem C* 116(50):26214–26221. doi:[10.1021/jp309321w](https://doi.org/10.1021/jp309321w)
- Mehdi BL, Gu M, Parent LR, Xu W, Nasybulin EN, Chen X, Unocic RR, Xu P, Welch DA, Abellan P, Zhang JG, Liu J, Wang CM, Arslan I, Evans J, Browning ND (2014) In-situ electrochemical transmission electron microscopy for battery research. *Microsc Microanal* 20(2):484–492. doi:[10.1017/S1431927614000488](https://doi.org/10.1017/S1431927614000488)
- Mehdi BL, Qian J, Nasybulin E, Park C, Welch DA, Faller R, Mehta H, Henderson WA, Xu W, Wang CM, Evans JE, Liu J, Zhang JG, Mueller KT, Browning ND (2015) Observation and quantification of nanoscale processes in lithium batteries by operando electrochemical (S)TEM. *Nano Lett* 15(3):2168–2173. doi:[10.1021/acs.nanolett.5b00175](https://doi.org/10.1021/acs.nanolett.5b00175)
- Mendoza-Huizar LH, Rios-Reyes CH, Gómez-Villegas MG (2009) Zinc electrodeposition from chloride solutions onto glassy carbon electrode. *J Mex Chem Soc* 53(4):243–247
- Miyazaki K, Lee YS, Fukutsuka T, Abe T (2012) Suppression of dendrite formation of zinc electrodes by the modification of anion-exchange ionomer. *Electrochemistry* 80(10):725–727. doi:[10.5796/electrochemistry.80.725](https://doi.org/10.5796/electrochemistry.80.725)
- Mogi R, Inaba M, Iriyama Y, Abe T, Ogumi Z (2002a) In situ atomic force microscopy study on lithium deposition on nickel substrates at elevated temperatures. *J Electrochem Soc* 149(4):A385–A390. doi:[10.1149/1.1454138](https://doi.org/10.1149/1.1454138)
- Mogi R, Inaba M, Iriyama Y, Abe T, Ogumi Z (2002b) Surface film formation on nickel electrodes in a propylene carbonate solution at elevated temperatures. *J Power Sources* 108:163–173
- Mogi R, Inaba M, Jeong S-K, Iriyama Y, Abe T, Ogumi Z (2002c) Effects of some organic additives on lithium deposition in propylene carbonate. *J Electrochem Soc* 149(12):A1578–A1583. doi:[10.1149/1.1516770](https://doi.org/10.1149/1.1516770)
- Monroe C, Newman J (2003) Dendrite growth in lithium/polymer systems: a propagation model for liquid electrolytes under galvanostatic conditions. *J Electrochem Soc* 150(10):A1377–A1384. doi:[10.1149/1.1606686](https://doi.org/10.1149/1.1606686)
- Monroe C, Newman J (2004) The effect of interfacial deformation on electrodeposition kinetics. *J Electrochem Soc* 151(6):A880–A886. doi:[10.1149/1.1710893](https://doi.org/10.1149/1.1710893)

- Monroe C, Newman J (2005) The impact of elastic deformation on deposition kinetics at lithium/polymer interfaces. *J Electrochem Soc* 152(2):A396–A404. doi:[10.1149/1.1850854](https://doi.org/10.1149/1.1850854)
- Morigaki K-I (2002) Analysis of the interface between lithium and organic electrolyte solution. *J Power Sources* 104:13–23
- Morigaki K-I, Ohta A (1998) Analysis of the surface of lithium in organic electrolyte by atomic force microscopy, fourier transform infrared spectroscopy and scanning auger electron microscopy. *J Power Sources* 76:159–166
- Nagao M, Hayashi A, Tatsumisago M, Kanetsuku T, Tsuda T, Kuwabata S (2013) In situ SEM study of a lithium deposition and dissolution mechanism in a bulk-type solid-state cell with a Li2S-P2S5 solid electrolyte. *Phys Chem Chem Phys* 15(42):18600–18606. doi:[10.1039/c3cp51059j](https://doi.org/10.1039/c3cp51059j)
- Naoi K, Mori M, Shinagawa Y (1996) Study of deposition and dissolution processes of lithium in carbonate-based solutions by means of the quartz-crystal microbalance. *J Electrochem Soc* 143(8):2517–2522
- Naoi K, Mori M, Naruoka Y, Lamanna WM, Atanasoski R (1999) The surface film formed on a lithium metal electrode in a new imide electrolyte, lithium Bis(perfluoroethylsulfonylimide) [LiN(C2F5SO2)2]. *J Electrochem Soc* 146(2):462–469
- Naudin C, Bruneel JL, Chami M, Desbat B, Grondin J, Lassègues JC, Servant L (2003) Characterization of the lithium surface by infrared and raman spectroscopies. *J Power Sources* 124(2):518–525. doi:[10.1016/s0378-7753\(03\)00798-5](https://doi.org/10.1016/s0378-7753(03)00798-5)
- Nazri G, Muller RH (1985a) In situ X-Ray diffraction of surface layers on lithium in nonaqueous electrolyte. *J Electrochem Soc* 132(6):1385–1387
- Nazri G, Muller RH (1985b) Composition of surface layers on Li electrodes in PC, LiClO4 of very low water content. *J Electrochem Soc* 132(9):2050–2054
- Nazri G, Muller RH (1985c) Effect of residual water in propylene carbonate on films formed on lithium. *J Electrochem Soc* 132(9):2054–2058
- Neudecker BJ, Dudney NJ, Bates JB (2000) “Lithium-Free” thin-film battery with in situ plated Li anode. *J Electrochem Soc* 147(2):517–523
- Nishida T, Nishikawa K, Rosso M, Fukunaka Y (2013) Optical observation of Li dendrite growth in ionic liquid. *Electrochim Acta* 100:333–341. doi:[10.1016/j.electacta.2012.12.131](https://doi.org/10.1016/j.electacta.2012.12.131)
- Nishikawa K, Fukunaka Y, Sakka T, Ogata YH, Selman JR (2007) Measurement of concentration profiles during electrodeposition of Li metal from LiPF6-PC electrolyte solution. *J Electrochem Soc* 154(10):A943–A948. doi:[10.1149/1.2767404](https://doi.org/10.1149/1.2767404)
- Nishikawa K, Mori T, Nishida T, Fukunaka Y, Rosso M, Homma T (2010) In situ observation of dendrite growth of electrodeposited Li metal. *J Electrochem Soc* 157(11):A1212–A1217. doi:[10.1149/1.3486468](https://doi.org/10.1149/1.3486468)
- Nishikawa K, Mori T, Nishida T, Fukunaka Y, Rosso M (2011) Li dendrite growth and Li⁺ ionic mass transfer phenomenon. *J Electroanal Chem* 661(1):84–89. doi:[10.1016/j.jelechem.2011.06.035](https://doi.org/10.1016/j.jelechem.2011.06.035)
- Nishikawa K, Naito H, Kawase M, Nishida T (2012) Morphological variation of electrodeposited Li in ionic liquid. *ECS Trans* 41:3–10
- Odziemkowski M, Krell M, Irish DE (1992) A raman microprobe in situ and ex situ study of film formation at lithium/organic electrolyte interfaces. *J Electrochem Soc* 139(11):3052–3063
- Orsini F, Du Pasquier A, Beaudoin B, Tarascon JM, Trentin M, Langenhuizen N, De Beer E, Notten P (1998) In situ scanning electron microscopy (SEM) observation of interfaces within plastic lithium batteries. *J Power Sources* 76:19–29
- Orsini F, du Pasquier A, Beaudouin B, Tarascon JM, Trentin M, Langenhuizen N, de Beer E, Notten P (1999) In situ SEM study of the interfaces in plastic lithium cells. *J Power Sources* 81–82:918–921. doi:[10.1016/S0378-7753\(98\)00241-9](https://doi.org/10.1016/S0378-7753(98)00241-9)
- Osaka T, Homma T, Momma T, Yarimizu H (1997a) In situ observation of lithium deposition processes in solid polymer and gel electrolytes. *J Electroanal Chem* 421:153–156
- Osaka T, Momma T, Matsumoto Y, Uchida Y (1997b) Surface characterization of electrodeposited lithium anode with enhanced cycleability obtained by CO₂ addition. *J Electrochem Soc* 144(5):1709–1713

- Ota H, Wang X, Yasukawa E (2004a) Characterization of lithium electrode in lithium imides/ethylene carbonate, and cyclic ether electrolytes. I. Surface morphology and lithium cycling efficiency. *J Electrochem Soc* 151(3):A427–A436. doi:[10.1149/1.1644136](https://doi.org/10.1149/1.1644136)
- Ota H, Shima K, Ue M, Yamaki J-I (2004b) Effect of vinylene carbonate as additive to electrolyte for lithium metal anode. *Electrochim Acta* 49(4):565–572. doi:[10.1016/j.electacta.2003.09.010](https://doi.org/10.1016/j.electacta.2003.09.010)
- Ota H, Sakata Y, Wang X, Sasahara J, Yasukawa E (2004c) Characterization of lithium electrode in lithium imides/ethylene carbonate and cyclic ether electrolytes. II. Surface chemistry. *J Electrochem Soc* 151(3):A437–A446. doi:[10.1149/1.1644137](https://doi.org/10.1149/1.1644137)
- Qian J, Xu W, Bhattacharya P, Engelhard M, Henderson WA, Zhang Y, Zhang J-G (2015a) Dendrite-free Li deposition using trace-amounts of water as an electrolyte additive. *Nano Energy* 15:135–144. doi:[10.1016/j.nanoen.2015.04.009](https://doi.org/10.1016/j.nanoen.2015.04.009)
- Qian J, Henderson WA, Xu W, Bhattacharya P, Engelhard M, Borodin O, Zhang JG (2015b) High rate and stable cycling of lithium metal anode. *Nat Commun* 6:6362. doi:[10.1038/ncomms7362](https://doi.org/10.1038/ncomms7362)
- Rey I, Lassègues JC, Baudry P, Majastre H (1998a) Study of a lithium battery by confocal Raman microspectrometry. *Electrochim Acta* 43(10–11):1539–1544
- Rey I, Bruneel J-L, Grondin J, Servant L, Lassègues J-C (1998b) Raman spectroelectrochemistry of a lithium/polymer electrolyte symmetric cell. *J Electrochem Soc* 145(9):3034–3042
- Rosso M, Gobron T, Brissot C, Chazalviel JN, Lascaud S (2001) Onset of dendritic growth in lithium/polymer cells. *J Power Sources* 97–98:804–806
- Rosso M, Brissot C, Teyssot A, Dollé M, Sannier L, Tarascon J-M, Bouchet R, Lascaud S (2006) Dendrite short-circuit and fuse effect on Li/polymer/Li cells. *Electrochim Acta* 51(25):5334–5340. doi:[10.1016/j.electacta.2006.02.004](https://doi.org/10.1016/j.electacta.2006.02.004)
- Ryou M-H, Lee DJ, Lee J-N, Lee YM, Park J-K, Choi JW (2012) Excellent cycle life of lithium-metal anodes in lithium-ion batteries with mussel-inspired polydopamine-coated separators. *Adv Energy Mater* 2(6):645–650. doi:[10.1002/aenm.201100687](https://doi.org/10.1002/aenm.201100687)
- Sacci RL, Dudney NJ, More KL, Parent LR, Arslan I, Browning ND, Unocic RR (2014) Direct visualization of initial SEI morphology and growth kinetics during lithium deposition by in situ electrochemical transmission electron microscopy. *Chem Commun* 50(17):2104–2107. doi:[10.1039/c3cc49029g](https://doi.org/10.1039/c3cc49029g)
- Sagane F, Ikeda K-I, Okita K, Sano H, Sakaebe H, Iriyama Y (2013) Effects of current densities on the lithium plating morphology at a lithium phosphorus oxynitride glass electrolyte/copper thin film interface. *J Power Sources* 233:34–42. doi:[10.1016/j.jpowsour.2013.01.051](https://doi.org/10.1016/j.jpowsour.2013.01.051)
- Sano H, Sakaebe H, Matsumoto H (2011) Observation of electrodeposited lithium by optical microscope in room temperature ionic liquid-based electrolyte. *J Power Sources* 196(16):6663–6669. doi:[10.1016/j.jpowsour.2010.12.023](https://doi.org/10.1016/j.jpowsour.2010.12.023)
- Sawada Y, Dougherty A, Gollub JP (1986) Dendritic and fractal patterns in electrolytic metal deposits. *Phys Rev Lett* 56(12):1260–1263. doi:[10.1103/PhysRevLett.56.1260](https://doi.org/10.1103/PhysRevLett.56.1260)
- Selim R, Bro P (1974) Some observations on rechargeable lithium electrodes in a propylene carbonate electrolyte. *J Electrochem Soc* 121(11):1457–1459
- Shiraishi S, Kanamura K (1998) The observation of electrochemical dissolution of lithium metal using electrochemical quartz crystal microbalance and in-situ tapping mode atomic force microscopy. *Langmuir* 14:7082–7086
- Shiraishi S, Kanamura K, Zi Takehara (1999) Surface condition changes in lithium metal deposited in nonaqueous electrolyte containing HF by dissolution-deposition cycles. *J Electrochem Soc* 146(5):1633–1639
- Shiraishi S, Kanamura K, Takehara Z-I (2001) Imaging for uniformity of lithium metal surface using tapping mode-atomic force and surface potential microscopy. *J Phys Chem B* 105:123–134
- Stark JK, Ding Y, Kohl PA (2011) Dendrite-free electrodeposition and reoxidation of lithium-sodium alloy for metal-anode battery. *J Electrochem Soc* 158(10):A1100–A1105. doi:[10.1149/1.3622348](https://doi.org/10.1149/1.3622348)

- Stark JK, Ding Y, Kohl PA (2013) Nucleation of electrodeposited lithium metal: dendritic growth and the effect of co-deposited sodium. *J Electrochem Soc* 160(9):D337–D342. doi:[10.1149/2.028309jes](https://doi.org/10.1149/2.028309jes)
- Steiger J (2015) Mechanisms of dendrite growth in lithium metal batteries. PhD Thesis, Karlsruhe Institute of Technology (KIT), Germany
- Steiger J, Kramer D, Mönig R (2014a) Mechanisms of dendritic growth investigated by in situ light microscopy during electrodeposition and dissolution of lithium. *J Power Sources* 261:112–119. doi:[10.1016/j.jpowsour.2014.03.029](https://doi.org/10.1016/j.jpowsour.2014.03.029)
- Steiger J, Kramer D, Mönig R (2014b) Microscopic observations of the formation, growth and shrinkage of lithium moss during electrodeposition and dissolution. *Electrochim Acta* 136:529–536. doi:[10.1016/j.electacta.2014.05.120](https://doi.org/10.1016/j.electacta.2014.05.120)
- Steiger J, Richter G, Wenk M, Kramer D, Mönig R (2015) Comparison of the growth of lithium filaments and dendrites under different conditions. *Electrochem Commun* 50:11–14. doi:[10.1016/j.elecom.2014.11.002](https://doi.org/10.1016/j.elecom.2014.11.002)
- Tang M, Albertus P, Newman J (2009) Two-dimensional modeling of lithium deposition during cell charging. *J Electrochem Soc* 156(5):A390–A399. doi:[10.1149/1.3095513](https://doi.org/10.1149/1.3095513)
- Teyssot A, Belhomme C, Bouchet R, Rosso M, Lascaud S, Armand M (2005) Inter-electrode in situ concentration cartography in lithium/polymer electrolyte/lithium cells. *J Electroanal Chem* 584(1):70–74. doi:[10.1016/j.jelechem.2005.01.037](https://doi.org/10.1016/j.jelechem.2005.01.037)
- Thompson RS, Schroeder DJ, López CM, Neuhold S, Vaughey JT (2011) Stabilization of lithium metal anodes using silane-based coatings. *Electrochem Commun* 13(12):1369–1372. doi:[10.1016/j.elecom.2011.08.012](https://doi.org/10.1016/j.elecom.2011.08.012)
- Voss RF, Tomkiewicz M (1985) Computer simulation of dendritic electrodeposition. *J Electrochem Soc* 132(2):371–375
- Wang X, Yasukawa E, Kasuya S (2000) Lithium imide electrolytes with two-oxygen-atom-containing cycloalkane solvents for 4 V lithium metal rechargeable batteries. *J Electrochem Soc* 147(7):2421–2426
- Wenzel S, Leichtweiss T, Krüger D, Sann J, Janek J (2015) Interphase formation on lithium solid electrolytes—an in situ approach to study interfacial reactions by photoelectron spectroscopy. *Solid State Ionics* 278:98–105. doi:[10.1016/j.ssi.2015.06.001](https://doi.org/10.1016/j.ssi.2015.06.001)
- Yamaki J-I, Tobishima S-I, Hayashi K, Saito K, Nemoto Y, Arakawa M (1998) A consideration of the morphology of electrochemically deposited lithium in an organic electrolyte. *J Power Sources* 74:219–227
- Yang L, Smith C, Patrisi C, Schumacher CR, Lucht BL (2008) Surface reactions and performance of non-aqueous electrolytes with lithium metal anodes. *J Power Sources* 185(2):1359–1366. doi:[10.1016/j.jpowsour.2008.09.037](https://doi.org/10.1016/j.jpowsour.2008.09.037)
- Yoon S, Lee J, Kim S-O, Sohn H-J (2008) Enhanced cyclability and surface characteristics of lithium batteries by Li–Mg co-deposition and addition of HF acid in electrolyte. *Electrochim Acta* 53(5):2501–2506. doi:[10.1016/j.electacta.2007.10.019](https://doi.org/10.1016/j.electacta.2007.10.019)
- Yoshimatsu I, Hirai T, Yamaki J-I (1988) Lithium electrode morphology during cycling in lithium cells. *J Electrochem Soc* 135(10):2422–2427
- Zhamu A, Chen G, Liu C, Neff D, Fang Q, Yu Z, Xiong W, Wang Y, Wang X, Jang BZ (2012) Reviving rechargeable lithium metal batteries: enabling next-generation high-energy and high-power cells. *Energy Environ Sci* 5(2):5701–5707. doi:[10.1039/c2ee02911a](https://doi.org/10.1039/c2ee02911a)
- Zhang Y, Qian J, Xu W, Russell SM, Chen X, Nasybulin E, Bhattacharya P, Engelhard MH, Mei D, Cao R, Ding F, Cresce AV, Xu K, Zhang JG (2014) Dendrite-free lithium deposition with self-aligned nanorod structure. *Nano Lett* 14(12):6889–6896. doi:[10.1021/nl5039117](https://doi.org/10.1021/nl5039117)
- Zinigrad E, Aurbach D, Dan P (2001) Simulation of galvanostatic growth of polycrystalline Li deposits in rechargeable Li batteries. *Electrochim Acta* 46:1863–1869

Lithium Metal Anodes and Rechargeable Lithium Metal
Batteries

Zhang, J.-G.; Xu, W.; Henderson, W.A.

2017, XV, 194 p. 94 illus., 39 illus. in color., Hardcover

ISBN: 978-3-319-44053-8